The centrosomal protein 83 (CEP83) regulates human pluripotent stem cell differentiation towards the kidney lineage

Fatma Mansour[1,2,3], Christian Hinze[1,2,4,5], Narasimha Swamy Telugu[4,6], Jelena Kresoja[7], Iman B. Shaheed[3], Christian Mosimann[7], Sebastian Diecke[4,5], Kai M. Schmidt-Ott[1,2,5*]

[1] Department of Nephrology and Medical Intensive Care, Charité–Universitätsmedizin Berlin, 12203 Berlin, Germany.

[2] Molecular and Translational Kidney Research, Max-Delbrück-Center for Molecular Medicine in the Helmholtz Association (MDC), 13125 Berlin, Germany

[3] Department of Pathology, Faculty of Veterinary Medicine, Cairo University, 12613 Giza, Egypt

[4] Berlin Institute of Health, Anna-Louisa-Karsch-Straße 2, 10178 Berlin, Germany

[5] Department of Nephrology and Hypertension, Hannover Medical School,30625 Hannover, Germany

[6] Technology Platform Pluripotent Stem Cells, Max Delbrück Center for Molecular Medicine in the Helmholtz Association (MDC), Robert-Rössle-Str. 10, 13092 Berlin, Germany

[7] University of Colorado School of Medicine, Anschutz Medical Campus, Department of Pediatrics, Section of Developmental Biology, 12801 E 17th Avenue, Aurora, CO 80045, USA

*Correspondence: Prof. Dr. Kai M. Schmidt-Ott, Department of Nephrology and Medical Intensive Care, Charité–Universitätsmedizin Berlin, corporate member of Freie Universität Berlin, Humboldt-Universität Berlin, 12203 Berlin, Germany. Kai.schmidt-ott@charite.de

Abstract

Background

During embryonic development, the mesoderm undergoes patterning into diverse lineages including axial, paraxial, and lateral plate mesoderm (LPM). Within the LPM, the so-called intermediate mesoderm (IM) forms kidney and urogenital tract progenitor cells, while remaining LPM forms cardiovascular, hematopoietic, mesothelial and additional progenitor cells. The signals that regulate these early lineage decisions are incompletely understood. Here, we found that the centrosomal protein 83 (CEP83), a centriolar component necessary for primary cilia formation and mutated in pediatric kidney disease, influences the differentiation of human induced pluripotent stem cells (hiPSCs) towards intermediate mesoderm.

Methods

We induced inactivating deletions of *CEP83* in hiPSCs and applied a 7 day in vitro protocol of intermediate mesoderm kidney progenitor differentiation, based on timed application of WNT and FGF agonists. We characterized induced mesodermal cell populations using single cell and bulk transcriptomics and tested their ability to form kidney structures in subsequent organoid culture.

Results

While hiPSCs with homozygous *CEP83* inactivation were normal regarding morphology and transcriptome, their induced differentiation into IM progenitor cells was perturbed.

Mesodermal cells induced after 7 days of monolayer culture of *CEP83*-deficient hiPCS exhibited absent or elongated primary cilia, displayed decreased expression of critical IM genes (*PAX8*, *EYA1*, *HOXB7*) and an aberrant induction of LPM markers (e. g. *FOXF1*, *FOXF2*, *FENDRR*, *HAND1*, *HAND2*). Upon subsequent organoid culture, wildtype cells differentiated to form kidney tubules and glomerular-like structures, whereas *CEP83*-deficient cells failed to generate kidney cell types, instead upregulating cardiomyocyte, vascular, and more general LPM progenitor markers.

Conclusion

Our data suggest that *CEP83* regulates the balance of intermediate mesoderm and lateral plate mesoderm formation from human pluripotent stem cells, identifying a potential link between centriolar or ciliary function and mesodermal lineage induction.

Keywords: distal appendages; Centrosomal protein 83; kidney development; pluripotent stem cells; kidney organoids; primary cilium; CRISPR-cas9

Introduction

During mammalian embryonic development, the mesoderm forms axial, paraxial, and lateral plate domains that harbor precursor cells for distinct organ systems. Forming as a major part of the lateral plate mesoderm (LPM), the intermediate mesoderm (IM) harbors progenitor cells of all kidney epithelial cells[1], whereas remaining LPM contributes progenitors of various cell types, including cells of the cardiovascular system[2]. The molecular and cellular mechanisms that drive induction of the IM and distinct LPM domains during embryonic development are not fully understood.

The centrosomal protein 83 (CEP83) is a component of distal appendages (DAPs) of centrioles. DAPs are involved in the anchoring of the mother centriole to the cell membrane, an early and critical step in ciliogenesis[3-11]. CEP83 recruits other DAP components to the ciliary base, and loss of CEP83 disrupts ciliogenesis[4]. In radial glial progenitors, removal of CEP83 disrupts DAP assembly, and impairs the anchoring of the centrosome to the apical membrane as well as primary ciliogenesis[5,10]. Mutations of CEP83 in humans have been associated with infantile nephronophthisis[9], an early onset kidney disease that results in end stage renal disease before the age of 3 years[12,13] and additional organ anomalies[9]. To date, how loss of CEP83 function contributes to aberrant kidney development remains unclear.

Human induced pluripotent stem cells (iPSCs) provide useful tools to study molecular mechanisms of cellular differentiation. Protocols for the induction of kidney organoids from iPSC have been successfully developed[14-19]. The protocol by Takasato *et al*. uses stepwise exposure of iPSC to WNT and FGF agonists in a monolayer culture system for a 7 day period, which results in the induction of cells with a transcriptional

phenotype resembling kidney progenitors in the IM[17]. Transfer of these cells to an organoid culture system followed by another series of WNT and FGF signals results in differentiation of 3-dimensional kidney organoids composed of different kidney cells types, including glomerular and tubular cells. Genome editing studies have previously been used to study the effects of genetic defects associated with kidney diseases on kidney differentiation in human iPSC systems [18,20-24]. Here, we studied the effect of an induced knockout of *CEP83* in human iPSCs on kidney organoid differentiation. We uncovered a novel role of CEP83 in determining the balance of IM versus LPM differentiation, implicating a centrosomal protein in early mesodermal lineage decisions.

Concise Methods

hiPSCs cell line.

We used the human iPSC cell line BIHi005-A, which was generated by the Berlin Institute of Health (BIH). The hiPSCs were maintained in 6-well plates (Corning®, 353046) coated with Matrigel (Corning®, 354277) and cultured in Essential 8 medium (E8, A1517001, Gibco-Thermo Fisher Scientific) supplemented with 10µM Y-27632 (Rocki, Wako, 253-00513).

CRISPR CAS9 Technology to generate CEP83$^{-/-}$ hiPSCs clones.

Clustered Regularly Interspaced Short Palindromic Repeats (CRISPR)-Cas9 technology was used to generate *CEP83*$^{-/-}$ hiPSCs clones. We designed two CRISPR RNAs (crRNAs) (5'-GGCTGAAGTAGCGGAATTAA-AGG-3' and 5'-AAGAATACAGGTGCGGCAGT-TGG-3') using CRISPOR software[25]. The two crRNAs

were annealed with trans-activating CRISPR RNA (tracrRNA) to form two guide RNAs (gRNA1 and gRNA2) and then formed a RNP complex by incubating gRNA1 and gRNA2 separately with Alt-R® S.p. Cas9 Nuclease V3 (1 µM concentration, IDT, 1081058).The hiPSCs were transfected with RNP complexes using Neon transfection system (Thermo Fisher Scientific, MPK5000)[26] and Neon™ transfection 10 µl kit (Thermo Fisher Scientific, MPK10025) according to the manufacturer's instructions. After 48hrs of transfection, we analyzed the editing efficiency in the pool by PCR genotyping.

For PCR genotyping, we isolated genomic DNA from the pool of transfected cells followed by PCR using Phire™ Tissue Direct PCR Master Mix (Thermo Scientific, F170S) according to the manufacturer's instructions (**Figure 1B**). After confirming the editing efficiency in the pool, we generated single cell clones by the clonal dilution method. We plated 500 single cells per well of a 6 well plate and picked 24 clones using a picking hood S1 (Max Delbrück Centre Stem Cell Core Facility). Then, clones were screened for homozygous deletions of *CEP83* by PCR using Phire™ Tissue Direct PCR Master Mix. Selected knockout clones were further characterized for *CEP83* loss of function on the DNA, RNA, and protein level. *CEP83*$^{-/-}$ clones (*KO1, KO2*, and *KO3*) were registered as (BIHi005-A-71, BIHi005-A-72, and BIHi005-A-73) in the European Human Pluripotent Stem Cell Registry (https://hpscreg.eu).

Single nucleotide polymorphism (SNP)- Karyotype

To assess karyotype integrity, copy number variation (CNV) analysis on the human Illumina OMNI-EXPRESS-8v1.6 BeadChip was used. In brief, genomic DNA was isolated from three *WT* (*WT1, WT2*, and *WT3*) and three *KO* (*KO1*, *KO2* and *KO3*) clones using the DNeasy blood and tissue kit (Qiagen, Valencia, CA, United States), hybridized to the

human Illumina OMNI-EXPRESS-8v1.6 BeadChip (Illumina), stained, and scanned using the Illumina iScan system according to a standard protocol[27-29]. The genotyping was initially investigated using the GenomeStudio 1 genotyping module (Illumina). Following that, KaryoStudio 1.3 (Illumina) was used to perform automatic normalization and identify genomic aberrations in detected regions by generating B-allele frequency and smoothed Log R ratio plots. To detect copy number variations (CNVs), the stringency parameters were set to 75 kb (loss), 100 kb (gain), and CN-LOH (loss of heterozygosity). KaryoStudio generates reports and displays chromosome, length, list of cytobands, and genes in CNV-affected regions.

Differentiation Protocol.

We used the protocol of *Takasato* to differentiate the hiPSCs into nephron organoids[17]. Briefly, hiPSCs were cultured firstly in APEL2 medium (Stem Cell Technologies, 05270) supplemented with 5% Protein Free Hybridoma Medium II (PFHMII, GIBCO, 12040077), and 8 μM CHIR99021 (R&D, 4423/10) for 5 days, with medium changes every 2 days. Then, the cells were cultured in APEL2 medium supplemented with 200 ng/ml FGF9 (R&D, 273-F9-025) and 1 μg/ml heparin (Sigma Aldrich, H4784-250MG) for 2 days. On day 7, the cells were washed with 1X Dulbecco's PBS (DPBS, Thermo Fisher Scientific,14190-250), then trypsinized using trypsin EDTA-0.05% (Thermo Fisher Scientific, 25300-062) at 37 °C for 3 min. The cells were counted and divided to achieve 1×10^6 cells per organoid and cultured into 3D organoid culture on 0.4-μm-pore polyester membrane of Corning 6-well Transwell cell culture plate (Corning-Sigma Aldrich, CLS3450-24EA). Four to five organoids were seeded on one membrane using a P100

wide-bore tip, and cultured in APEL2 with 5 μM CHIR99021 at 37°C for 1h (CHIR99021 pulse). After the CHIR pulse, we changed the medium to APEL2 medium supplemented with 200 ng/ml FGF9 + 1 μg/ml heparin for 5 days with medium refreshing every 2d. The organoids were then cultured only in APEL2 medium with 1 μg/ml heparin for additional 13 days. The total differentiation time is 25 days (7+18).

DNA isolation and Polymerase Chain Reaction (PCR).

DNA was isolated from cells using DNeasy Blood & Tissue Kits (Qiagen, 69504). CEP83 primers were designed using Primer3 webtool (Table S1). PCR was done using Phusion high-fidelity DNA polymerase (Biolabs, New England, M0530) according to the manufacturer's instructions. PCR results were visualized on 1.5% agarose gel using a BioDoc Analyze dark hood and software system (Biometra).

RNA isolation, RNA Sequencing, and Quantitative PCR (qPCR).

Total RNA was isolated from the cells using RNAasy Mini Kit (QIAGEN, Hilden, Germany, 74104) following the manufacture instructions. The concentration, quality, and integrity of the extracted RNA were evaluated using Nanodrop (Thermo Scientific, Waltham, MA; USA), an Agilent 2100 Bioanalyzer, and the Agilent RNA 6000 Nano kit (Agilent Technologies, 5067-1511). 0.4 μg total RNA was used to obtain a poly A–enriched RNA library by Novogene (Cambridge, United Kingdom). Library concentration was performed using a Qubit fluorometer (HS RNA assay kit, Agilent Technologies). Library size was measured by Agilent 2100 bioanalyzer. The libraries were then subjected to 150-bp paired-end next-generation sequencing (Illumina NovaSeq 6000 S4 flow cells). Mutation visualization was performed using the Integrative Genomic Viewer (IGV) tool[30]. Read

194 counts of the sequenced RNA were normalized to Transcripts Per Million (TPM). The
195 TPM values of the variables were used to plot heatmaps and for principle cell analysis
196 (PCA) based on Pearson correlation, using self-written scripts in R (R Development Core
197 Team (2011)) (version 4.0.4).

198 RNA was reverse transcribed using the RevertAid First Strand cDNA Synthesis Kit
199 (Thermo Scientific). qPCR was performed using the FastStart Universal SYBR Green
200 Master (Rox) mix (Hoffmann-La Roche) according to the manufacturer's instructions.
201 Glyceraldehyde-3-Phosphate Dehydrogenase (*GAPDH*) mRNA expression and
202 calculated according to the ΔΔCt method. All primer pairs were designed using Primer3,
203 purchased at BioTeZ (Berlin, Germany), and sequences are shown in (Table S1).

204 **Single cell RNA sequencing (scRNA-seq)**

205 **Cells isolation and preparation**

206 Differentiated cells at day 7 were washed twice with 1X DPBS, dissociated with Accumax
207 solution, and resuspended in 1X DPBS. Then, cells were filtered, counted, and checked
208 for viability.

209 **Library preparation and single cell sequencing**

210 Single cell 3' RNA sequencing was performed using the 10x Genomics toolkit version
211 v3.1[31] according to the manufacturer's instructions aiming for 10000 cells. Obtained
212 libraries were sequenced on Illumina NextSeq 500 sequencers.

213 **Single-Cell Sequencing Data analysis and Clustering**

After sequencing and demultiplexing, fastq files were analyzed using Cellranger version 3.0.2. Gene expression matrices were then imported in R and Seurat objects were created using the Seurat R package (version 4.0.5)[32]. The gene expression matrices were initially filtered by applying lower and upper cut-offs for the number of detected genes (500 and 6000, respectively). The filtered data were then log normalized and scaled according to the number of unique molecular identifiers (UMIs). The normalized and scaled data derived from the four samples were then merged into one Seurat object. Clustering was performed using the first 20 principal components. We used the Seurat FindAllMarkers function to extract marker gene lists that differentiate between clusters with log fold-change threshold ±0.25 using only positive marker expressed in a minimum of 25 % of cells. Principal component analysis (PCA) was done using the first 20 principle components in R using the following libraries factoextra, FactoMineR, and ggplot2.

Protein extraction and Immunoblotting

Proteins were extracted from hiPSCs using radioimmunoprecipitation assay (RIPA) buffer (Sigma-Aldrich, R0278) as described in details in supplementary data. 30 µg protein in RIPA buffer were mixed with 1x reducing (10% b-mercaptoethanol) NuPAGE loading buffer (Life Technologies, Carlsbad, CA), loaded on a precast polyacrylamide NuPage 4-12% Bis-Tris protein gel (Invitrogen, Carlsbad, CA, USA), and blotted on 0.45 µm pore size Immobilon-P Polyvinylidene difluoride (PVDF) membrane (EMD Millipore, Billerica, MA; USA). The membrane was blocked in 5% bovine serum albumin for 1 h at room temperature and incubated overnight at 4°C with primary antibodies: Anti-CEP83 produced in rabbit (1:500, Sigma-Aldrich) and Anti-α-Tubulin produced in mouse (1:500, Sigma-Aldrich, T9026). Then, the membrane was incubated for 1 h at room temperature

with horseradish peroxidase-conjugated secondary antibodies (1:2000, Sigma-Aldrich, Saint Louis, MO, USA). Chemiluminescent reagent (Super Signal–West Pico; Thermo Scientific, Waltham, MA; USA) was used to detect the proteins. The spectra^{TM} Multicolor Broad Range Protein Ladder (Thermo Fisher Scientific, USA) was used to evaluate the molecular weight of corresponding protein bands.

Histology and Immunofluorescence (IF) staining

Cells at different time points were checked regularly under confocal microscope (Leica DMI 6000 CEL) for differentiation progress. Quantitative analysis of nephron-like structure formation within each organoid (D25) were done on tile scanning images of each organoid by estimating the percentage of the organoid area composed of nephron-like structures using 13 WT and 9 KO organoids. Organoids were fixed in BD Cytofix buffer (554655, BD Biosciences) for 1 hour on ice. Then organoids were gradually dehydrated in increasing ethanol concentrations, cleared in xylene, and embedded in paraffin. Organoids were cut into 3.5 µm-thick sections. The sections were deparaffinized, dehydrated, and stained in hematoxylin (Sigma-Aldrich, Saint Louis, MO) for 3 minutes and in 1% eosin (Sigma-Aldrich) for 2 minutes. For immunostaining, organoids were fixed with BD Cytofix, permeabilized with BD Perm/Wash (554723, BD Biosciences), and blocked with blocking solution (1% BSA + 0.3% triton-X-100 in 1X DPBS) for 2 h. Cells were incubated overnight at 4°C with primary antibodies (table S2), then incubated with fluorescence-labeled secondary antibodies with 1:500 dilution including Cy3, Cy5, Alexa488, and Alexa647 (Jackson ImmunoResearch, Newmarket, UK) and Cy3 Streptavidin (Vector lab, Burlingame, USA) overnight at 4°C. DAPI was then used for nuclear staining (Cell signaling Technology, Danvers, MA, USA) with 1:300000 dilution

for 1 hour at RT. Finally, cells were mounted with Dako fluorescent mounting medium (Agilent Technologies). Images were taken using a SP8 confocal microscope (Carl Zeiss GmbH, Oberkochen, Germany). Quantitative analyses of acquired images were performed using ImageJ software (1.48v; National Institutes of Health, Bethesda, MD).

Comparison to zebrafish lateral plate mesoderm (LPM)

The upregulated genes in CEP83$^{-/-}$ cells at day 7 and at day 25 were compared with the top 20 orthologous genes identified in subclusters of zebrafish LPM identified by scRNA-seq (Prummel et al., 2022), as deposited on ArrayExpress (E-MTAB-9727)[33].

Statistical analysis

scRNA-seq was done on two biological replicates representing two different clones of CEP83-/- and control cells, respectively. All other experiments were performed using three biological replicates representing three independent clones of *CEP83*$^{-/-}$ and control cells at different time points. A common excel sheet for the genes present in both bulk RNA and scRNA sequencing were generated in R. The sheet includes in total 20894 genes and represents the TPM values of both groups (*WT* and *KO*) on day 0, day7, day 25 of differentiation. The maximal TPM (TPMmax) and the minimum TPM (TPMmin) were calculated for each gene across all samples. Highly variable genes (HVGs) were calculated based on the ratio of TPMmax and TPMmin. For heatmaps and PCA analysis, the top 1000 HVGs were plotted with selection of TPMmax >2 for each gene. Deregulated (upregulated and downregulated) genes between *WT* and *KO* groups were selected with expression criteria of TPM >2, fold change > 1.5, and *P*-value calculated on log10 TPM < 0.05. The unpaired 2-tailed t-test was used to compare two groups. All graphs were

generated using GraphPad Prism 7.04 (GraphPad Software, San Diego, CA). Data are presented as mean ± SD.

Results

CEP83 is essential for the differentiation of human induced pluripotent stem cells into kidney cells

To investigate the effect of *CEP83* loss on the differentiation of hiPSCs into intermediate mesoderm (IM) kidney progenitors, we applied CRISPR-Cas9 technology to induce a null mutation in the *CEP83* gene in hiPSCs **(Figure1A)**. Three hiPSCs clones designated *CEP83*$^{-/-}$ (*KO1*, *KO2*, and *KO3*) carried deletions within *CEP83* exon 7, each of which led to an induction of a premature stop codon resulting in a predicted truncated protein **(Figure 1 B-D and Figure 1- figure supplement 1A)**. These clones exhibited a complete loss of CEP83 protein by immunoblotting **(Figure 1 E)**. Three wildtype clones were derived as controls (*WT1*, *WT2*, and *WT3*). All six clones were morphologically indistinguishable (by brightfield microscopy), and had similar overall gene expression profiles (by bulk RNA-seq and qRT-PCR), including pluripotency and lineage marker expression **(Figure 1- figure supplement 1B, C, and Figure 1- figure supplement 2A, B)**. In KO clones, the anticipated altered transcripts of CEP83 were detectable based on bulk RNA-seq (data not shown). Single nucleotide polymorphism (SNP) - analysis confirmed identical karyotypes of all six clones **(Figure 1- figure supplement 2C)**.

Together, these findings confirmed successful deletion of CEP83 in iPSCs without any overt direct cellular phenotypic consequences. We applied a 7 day monolayer protocol

using timed application of WNT and FGF agonists as reported by Takasato et al[17] to differentiate *WT* and *KO* hiPSCs into IM kidney progenitors[14-16] **(Figure 2A)**.

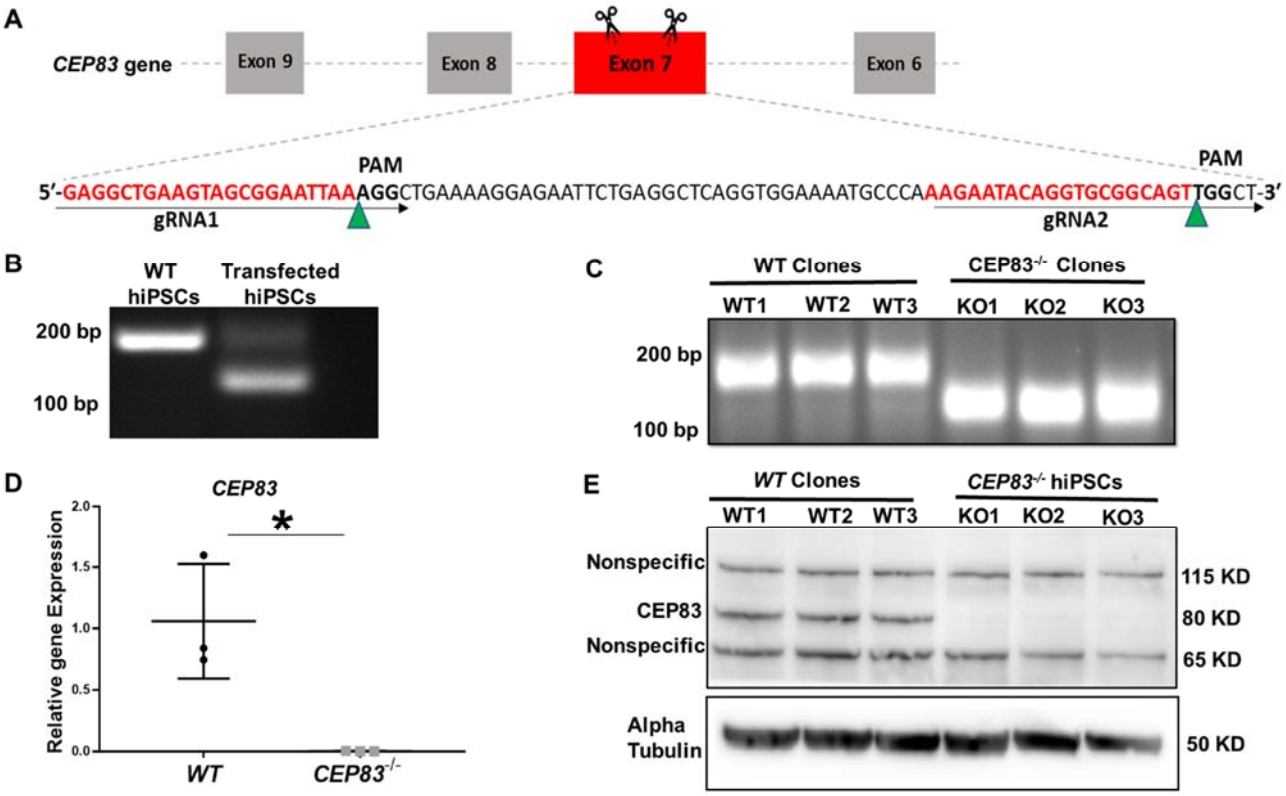

Figure 1: Generation of CEP83-deficient human pluripotent stem cells. (A) Schematic diagram of the experimental approach to induce a deleting mutation in exon 7 of the *CEP83* gene. Two guide RNAs (gRNAs) were designed to induce an approximately 63 bp deletion within exon 7 of the *CEP83* gene after non-homologous end joining. (B) Ribonucleoprotein (RNP) complex containing crispr RNAs (crRNAs), trans-activating crRNA (tracrRNA), and Cas9 endonuclease was transfected into hiPSCs by electroporation. DNA extracted from pooled transfected cells was subjected to PCR targeting the predicted deletion site in the *CEP83* gene. In addition to the 182 bp fragment present in untransfected wildtype (WT) cells, an approximately 120 bp fragment was detected in transfected cells, corresponding to the induced deletion in exon 7. Twenty-four single IPS cell-derived clones from these transfected cells were picked and cultured. (C) Three of these clones (*CEP83*$^{-/-}$ clones *KO1, KO2, KO3*) carried 62-74b bp deletions within *CEP83* exon 7, which led to an induction of premature stop codons or frameshift mutation on both alleles of *CEP83*. Three wildtype clones (*WT1, WT2,* and *WT3*) were used as controls. (D) Quantitative RT-PCR

for a fragment corresponding to the deleted region in *CEP83* exon 7 produced a detectable signal in RNA extracts from WT clones but not CEP83$^{-/-}$ clones. (E) Immunoblotting of *WT* and *CEP83*$^{-/-}$ clones using a CEP83 antibody targeting the C-terminal region of the protein (see methods for details) indicated a complete loss of the 83 kDa band corresponding to CEP83 protein in the three *KO* clones compared with the three *WT* clones. Data are mean ± SD.*P < 0.05 and **P < 0.01 vs. WT. See Figure 1- source data 1-2. See also Figure 1—figure supplements 1–2.

After 7 days of culture (D7), *WT* and *KO* cells exhibited an indistinguishable morphology by bright field microscopy **(Figure 2B, C)**. Immunostaining for acetylated tubulin, however, indicated abnormal primary cilia formation in *CEP83*-deficient cells **(Figure 2D, E).** The number of ciliated cells was reduced from approximately 30% (in *WT* clones) to less than 10% (in *KO* clones) **(Figure 2F)**. Among ciliated cells, the length of cilia was increased from 2-5 µm (in *WT* clones) to 5-13 µm (in *KO* clones) (**Figure 2G**). This indicated that *CEP83*$^{-/-}$ hiPSCs differentiated towards IM progenitors exhibited ciliary abnormalities. To analyze the induced IM kidney progenitor cells functionally, we collected D7 *WT* and *CEP83*$^{-/-}$ cells and placed them into an organoid culture system again applying timed WNT and FGF agonists to foster differentiation of mature kidney cell types, as previously reported[17] (**Figure 2A**). Organoids harvested from *WT* clones after a total of 25 days of culture (D25) had formed patterned kidney epithelial-like structures, including NPHS1-positive glomerulus-like structures, Lotus tetragonolobus lectin (LTL)-positive proximal tubule-like, and E-cadherin (E-cad)-positive distal tubule-like structures **(Figure 3A, C, E)**. In contrast, *CEP83*$^{-/-}$ organoids at day 25 were composed of monomorphic cells with a mesenchyme-like appearance, which stained negative for an array of kidney cell markers (**Figure 3B, D, and F**).

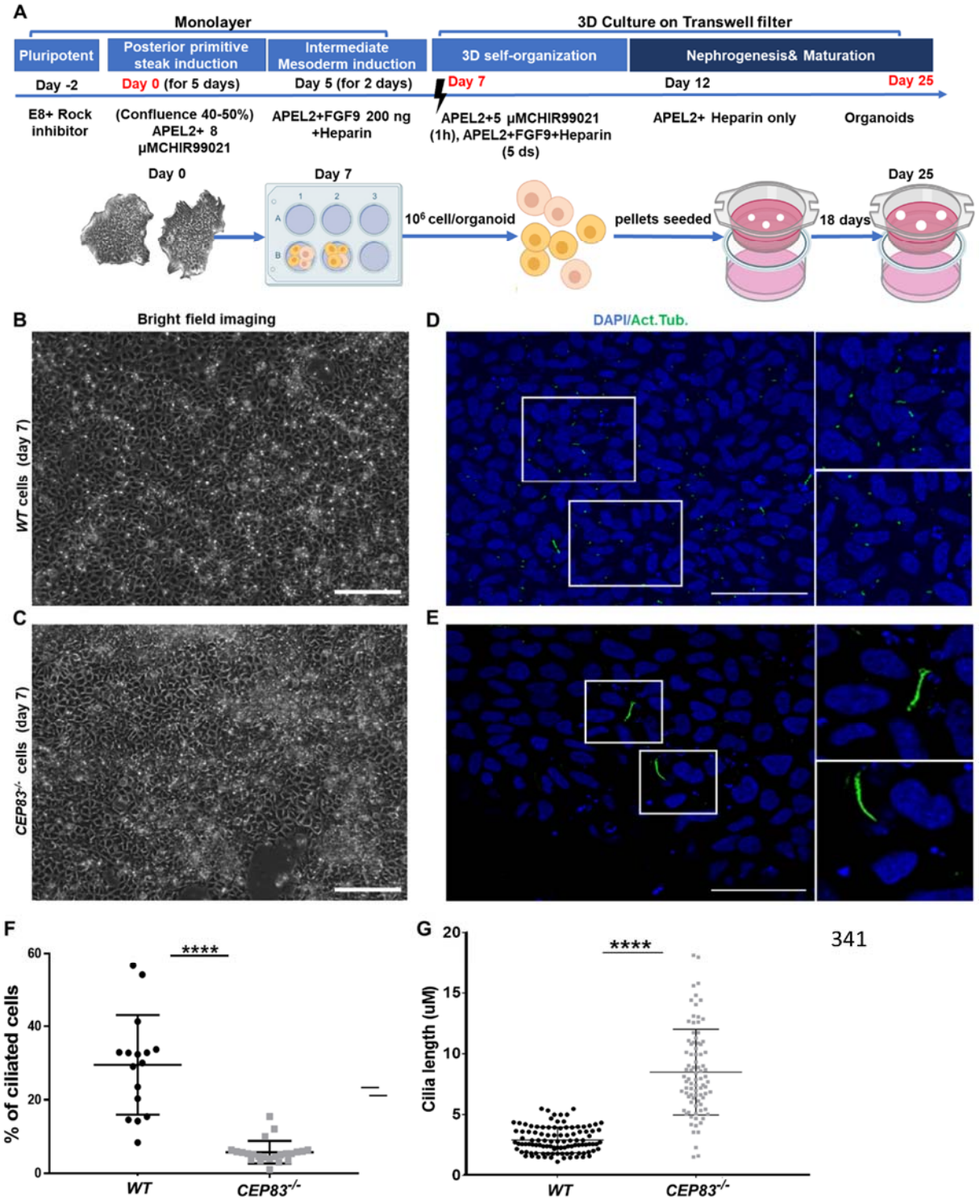

341

345 **Figure 2: Differentiation of CEP83$^{-/-}$ hiPSCs to intermediate mesoderm cells (day 7) is associated**
346 **with defective ciliogenesis.** (A) The schematic diagram illustrates the applied differentiation protocol of
347 hiPSCs, as previously described by Takasato *et al*.[34]. (B-C) *WT* and *CEP83*$^{-/-}$ cells on D7 of differentiation

did not show overt morphological differences by brighfield microscopy. (D-E) Representative images of *WT* and *CEP83*$^{-/-}$ cells on D7, immunostained for acetylated tubulin (green) and nuclei (DAPI, blue), revealing fewer and elongated cilia in *CEP83*$^{-/-}$ cells. (F) Quantitative analysis of the percentage of ciliated cells in *WT* and *CEP83*$^{-/-}$ cells (D7). (G) Quantitative analysis of the ciliary length in *WT* and *CEP83*$^{-/-}$ cells (D7). n = 3 clones per group. ****$P < 0.0001$. Bar = 50 μm. See Figure 2- figure supplement 1.

Kidney epithelial-like structures formed only in *WT*, but not in *CEP83*$^{-/-}$ organoids (**Figure 3G**). Similar to the findings in day 7 cells reported above, primary cilia were found in fewer cells of *CEP83*$^{-/-}$ organoids (<5% of cells) and were abnormally elongated (**Figure 2-figure supplement 1**).

Next, bulk RNA sequencing of *WT* (*WT1*, *WT2*, *WT3*) and *CEP83*$^{-/-}$ (KO1, KO2, KO3) organoids was carried out to evaluate differential gene expression on a genome-wide level, and RT-PCR was used to validate selected genes. Hierarchical clustering of the samples indicated strong gene expression differences between *WT* and *CEP83*$^{-/-}$ samples **(Figure 3- figure supplement 1)**. Several genes associated with kidney development and kidney epithelial differentiation were differentially expressed with high expression in *WT* organoids, but showed comparatively low or absent expression in *CEP83*$^{-/-}$ organoids: these genes included kidney-specific lineage genes (*PAX2*, *PAX8*), and lineage/differentiation markers of glomerular cells (*NPHS1*, *PODXL*, *WT1*, *PTPRO*), proximal (*HNF1B*, *LRP2*, *CUBN*) and distal (*EMX2*, *MAL2*, *EPCAM*, GATA3) kidney epithelial cells. **(Figure 3H-L, Figure 3- figure supplement 1B-H, and Figure 3- figure supplement 2).** This indicated that *CEP83*$^{-/-}$ IM progenitors failed to differentiate into kidney cells, suggesting that *CEP83* function is necessary to complete essential steps in the process of differentiation from pluripotent stem cells to kidney cells.

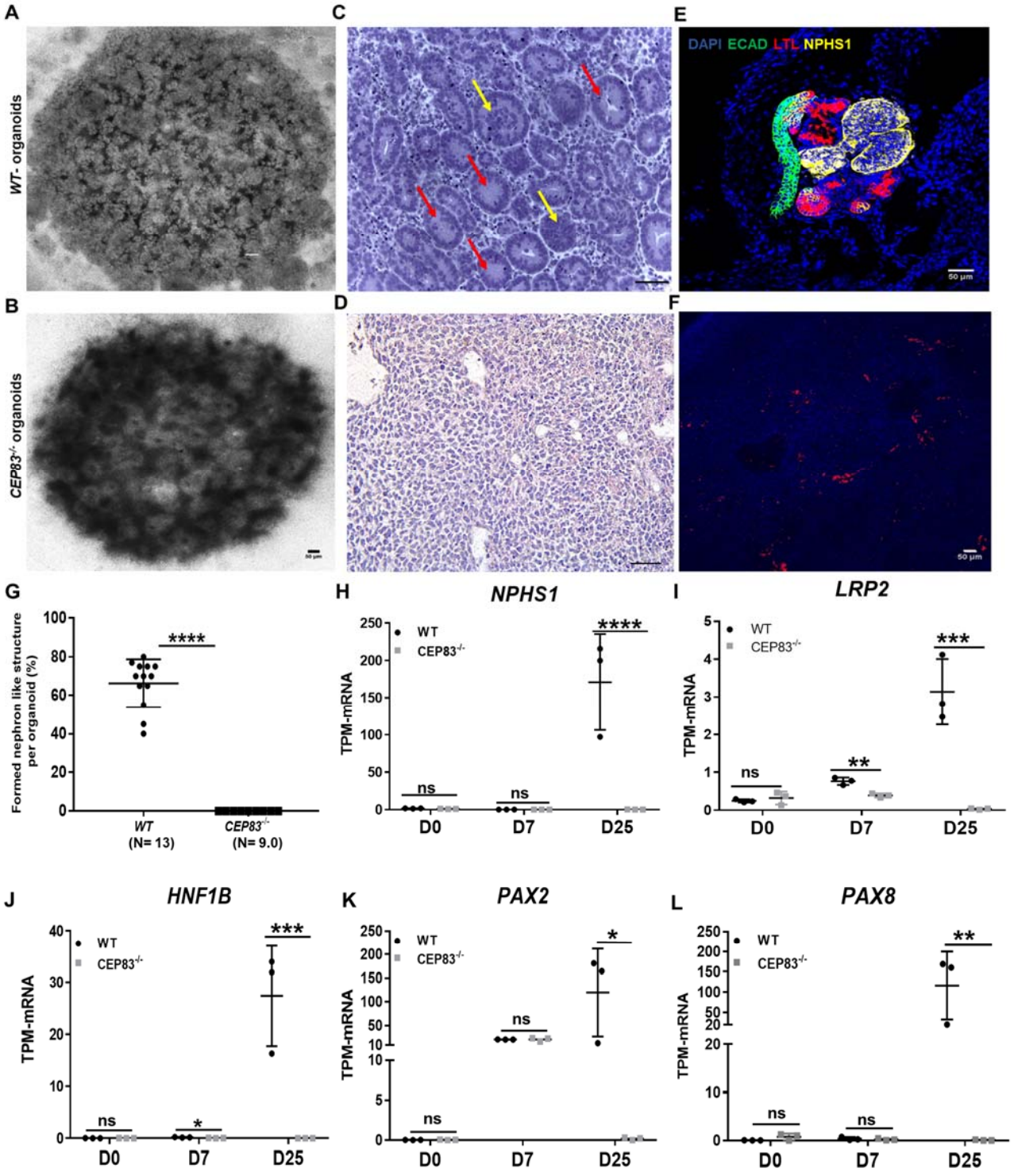

372 **Figure 3: Defective kidney organoid differentiation from *CEP83*-deficient pluripotent stem cells.** (A,
373 B) Bright-field images of organoids after a total of 25 days of culture (D25) indicate formation of multiple
374 kidney-like structures in *WT* organoids (A), whereas *CEP83*$^{-/-}$ organoids are composed of uniform clusters
375 (B). (C, D) Representative images of hematoxylin-eosin (HE)–stained sections of organoids. *WT* organoids

(C) display glomerulus-like (yellow arrows) and tubular (red arrow) components, whereas *CEP83*$^{-/-}$ organoids (D) are composed of monomorphic mesenchymal-like cells. (E-F) Whole mounting immunostaining of organoids for NPHS1 (podocyte marker), LTL (proximal tubule marker), and CDH1 (distal tubule marker) indicate segmented nephron-like structures in *WT* organoids (E) and absence of such structures in *CEP83*$^{-/-}$ organoids (F). (G) Quantitative analysis of brightfield images indicating the estimated percentage of organoid area composed of nephron like structures, organoids were collected from three different experiments. (H-L) Gene expression (transcripts per million, TPM) of *NPHP1* (H), *LRP2* (I), *HNF1B* (J), *PAX2* (K) and *PAX8* (L) in *WT* and *CEP83*$^{-/-}$ cells at the indicated time points based on bulk RNA sequencing. n= 3 clones per group. Data are mean ± SD. **P* < 0.05, ***P* < 0.01, ****P* < 0.001 and *****P* < 0.0001. ns= not significant. Panels B, C and D: Bar = 50 µm. See Figure 3- source data 1-2. See also Figure 3- figure supplements 1-2.

CEP83 deficiency associates with molecular defects of nephron progenitor cells

We next aimed to gain molecular insights into the lineage impact of *CEP83* deficiency during the course of kidney epithelial differentiation. Since no global transcriptomic differences were detectable between *WT* and *CEP83*$^{-/-}$ hiPSCs prior to differentiation (see above), we focussed on mesodermal cell stages induced at D7, which displayed mild overall gene expression differences between *WT* and *CEP83*-deficient cells as detected by bulk RNA sequencing **(Figure 4- figure supplements 1A, B, and Figure 4- figure supplement 2)**.

A marked upregulation of nephron progenitor marker genes (*GATA3*, *HOXB7*, *HOXD11*, *EYA1*)[35-42] was observed in both *WT* and *CEP83*$^{-/-}$ cells at day 7 (**Figure 4- figure supplement 3A-D**), suggesting that the differentiation path of pluripotent *CEP83*$^{-/-}$ cells to IM nephron progenitors was largely intact. To understand the potential molecular defects at the IM stage in more detail, we performed single-cell RNA (scRNA) sequencing

on D7 *WT* and *CEP83*$^{-/-}$ cells (representing two different hiPSC clones for each condition differentiated in two separate experiments). We obtained transcriptomes from 27,328 cells, representing clones *WT1* (experiment 1, 3,768 cells), *WT2* (experiment 2, 5,793 cells), *KO1* (experiment 1, 8,503 cells), and *KO2* (experiment 2, 9,264 cells). Principal component analysis (PCA) using pseudo-bulk expression data of the top 1000 highly variable genes indicated that the first major component (dimension 1, explaining 54% of expression variation) was driven by the genotype (*WT* vs. *KO*), while the second major component (dimension 2, explaining 51% of expression variation) was driven by a batch effect of the two experiments **(Figure 4A)**. We combined all cells and generated a Uniform Manifold Approximation and Projection (UMAP) plot uncovering 10 different cell states/clusters (0-9; **Figure 4B**). We identified marker genes for each cluster (**Figure 4C**), indicating that clusters 1, 3 and 4 represented kidney progenitors/nascent nephrons (expressing e. g. *PAX8*, *EYA1*, *HOXB7*) in different phases of the cell cycle. Other clusters represented as-of-yet uncharacterized cell types, which was consistent with previous single cell transcriptome analyses from iPSC-derived cells induced by the same induction protocol[43,44]. Each of the four samples (*WT1*, *WT2*, *KO1*, *and KO2*) contributed to each cluster (**Figure 4D**). We focussed on kidney progenitors (cluster 1, 3, 4) and found that a substantially lower percentage of *KO* cells (11.9-12.5%) contributed to cluster 1 when compared with *WT* cells (25.9-36.3%) (**Figure 5A**). In contrast, similar percentages of *WT* and *KO* cells were represented in kidney progenitor clusters 3 and 4 (**Figure 5B, C**). Differential gene expression analysis in these three clusters indicated significantly lower expression of kidney progenitor markers *PAX8*, *EYA1* and *HOXB7* in *KO* cells from clusters 1, 3, and 4 when compared to *WT* cells (**Figure 5 D, E, F; Figure 5- figure**

423 **supplement 1**). These results indicate that *CEP83* deficiency remained permissive with
424 initial kidney progenitor induction, but that these cells exhibited mild molecular defects
425 detectable by differential expression of kidney progenitor genes, which potentially
426 contributed to the failure of *CEP83*-deficient cells to further differentiate towards mature
427 kidney cell types.

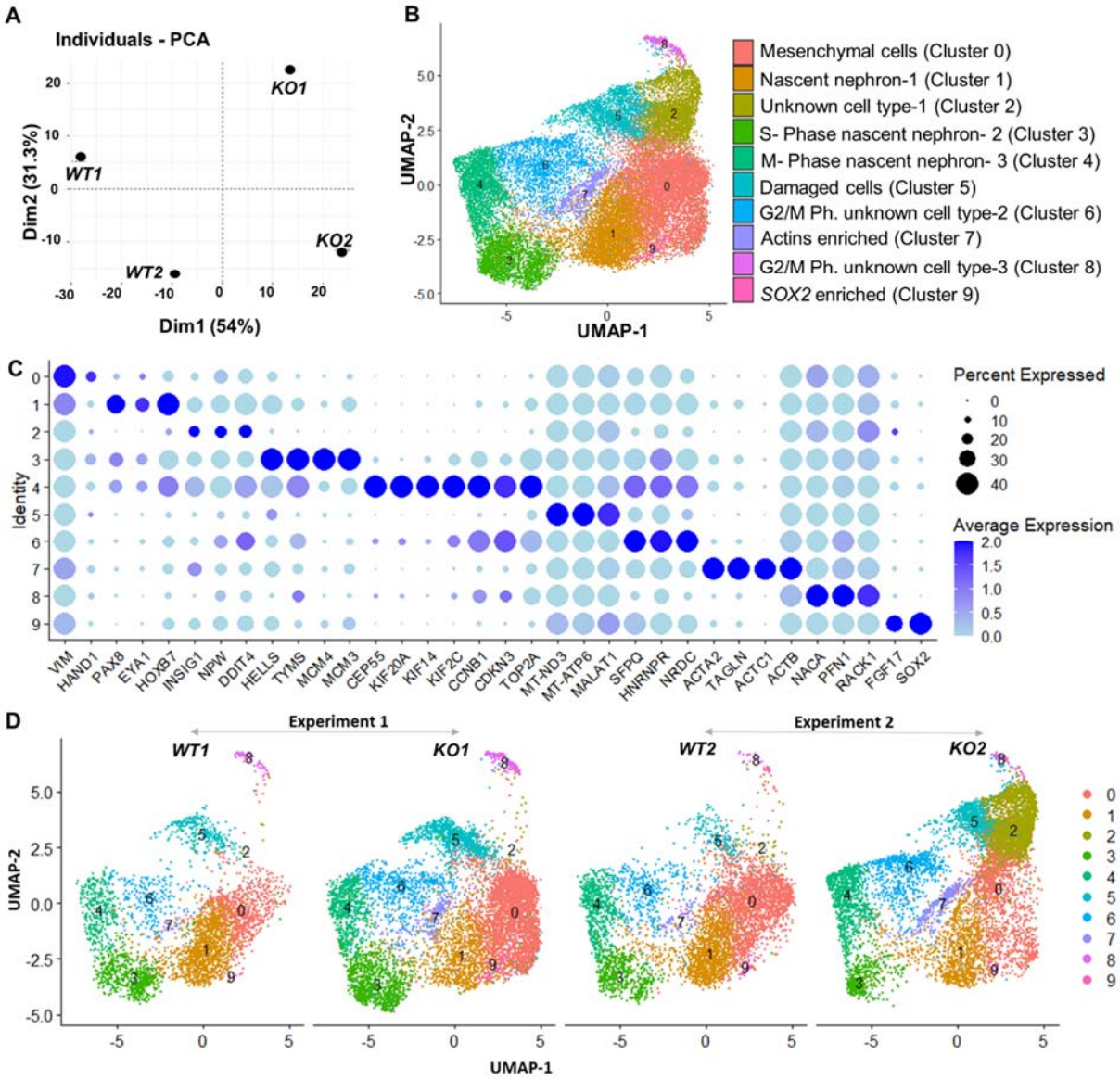

428 **Figure 4: Gene expression differences of WT and CEP83$^{-/-}$ D7 monolayers based on bulk and single**
429 **cell transcriptomics.** (A) Principal component analysis (PCA) of *WT* (*WT1, WT2*) and *CEP83*$^{-/-}$ (*KO1,*
430 *KO2*) cells at day 7 using the average gene expression of the top highly variable 1000 genes in pseudo-

bulk scRNA sequencing data. The % variation explained by each PCA axis is indicated in brackets. (B) PCA eigenvalues indicates that the principal components, Dim 1 (54%) and Dim 2 (31.3%), account for 85.3 % of the expression differences. Dim 1 separates the WT samples from the KO samples, while Dim 2 separates experiment 1 (*WT1, KO1*) from experiment 2 (*WT2, KO2*). (B) UMAP of scRNA-seq profiles from 27,328 cells from two wildtype clones (*WT1, WT2*) and two *CEP83*$^{-/-}$ clones (*KO1, KO2*) derived from two separate experiments (experiment 1: *WT1, KO1*; experiment 2: *WT2, KO2*). Unbiased clustering resulted in 10 clusters and (C) dot plot showing expression of selected marker genes of each cluster. (D) UMAP plots for *WT* and *KO* samples showing the distribution of all clusters per sample N=2 per group in B-D. See Figure 4- figure supplements 1-3. Source data is available as described in section (Data availability).

CEP83 deficiency promotes ectopic induction of lateral plate mesoderm-like cells followed by an expansion of cardiac and vascular progenitors

We next inspected single cell transcriptomes and bulk RNA sequencing data from D7 cells for genes that were up-regulated in *CEP83*$^{-/-}$ cells compared to WT cells. From this analysis, we observed a consistent upregulation of genes that are normally expressed in early lateral plate mesoderm (LPM), including *OSR1*, *FOXF1*, *FOXF2*, *FENDRR*, *HAND1*, *HAND2*, *CXCL12*, *GATA5*, and *GATA6*[45-69] (**Figure 6A-I**). This suggested that *CEP83*$^{-/-}$ cells entered an aberrant differentiation path assuming a phenotype indicative of broader LPM instead of more specific IM. To further substantiate this idea, we restricted the analysis to progenitor cells of clusters 1, 3, and 4 and to cells from cluster 0, which exhibited a mesenchymal transcriptome fingerprint (**see Figure 4C**). Within each cell, we analyzed the expression of LPM markers (*FOXF1*, *HAND1*, *HAND2*, and *CXCL12*) and of more restricted IM markers (*PAX8*, *EYA1*, *and HOXB7*) (**Figure 6- figure supplement 1**).

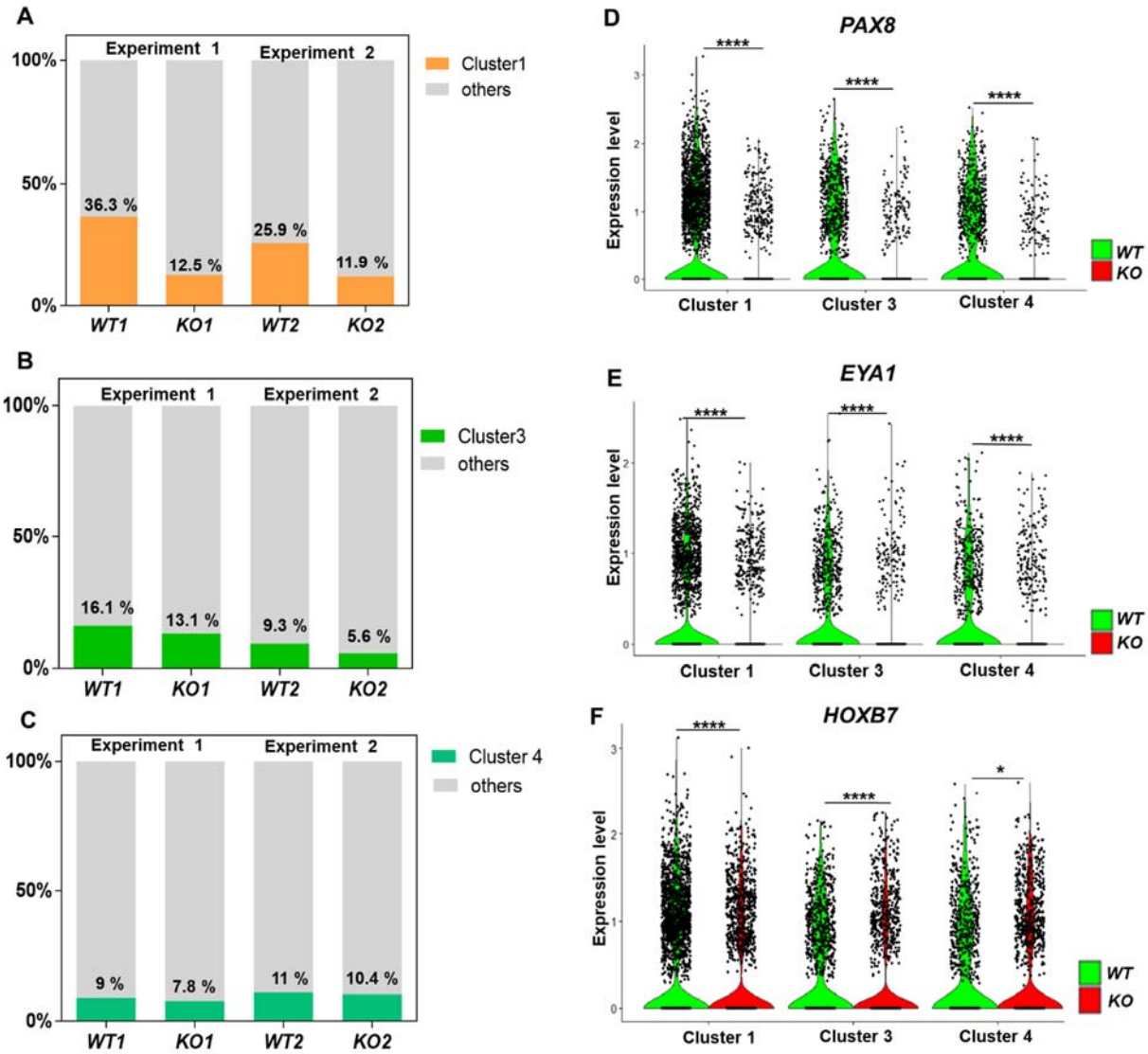

454 **Figure 5: Defective kidney progenitor differentiation from *CEP83*$^{-/-}$ cells after 7 days of monolayer**
455 **induction.** (A, B, C) Proportions of cells from kidney progenitor clusters 1 (A), 3 (B) and 4 (C) among
456 *wildtype* (*WT1, WT2*) and *CEP83*$^{-/-}$ (*KO1, KO2*) cells. (D, E, F) Violin plots of gene expression of kidney
457 progenitor genes *PAX8* (D), *EYA1* (E) and *HOXB7* (F) within kidney progenitor clusters 1, 3 and 4
458 comparing wildtype (*WT*) and *CEP83*$^{-/-}$ (*KO*) cells. N= 2 per group. *$P < 0.05$ and ****$P < 0.0001$. Figure 5-
459 figure supplement 1. Source data is available as described in section (Data availability).

460 This analysis indicated that *WT* cells of these clusters exhibited an IM-like phenotype,
461 while *KO* cells were shifted towards an LPM-like phenotype. The common IM/LPM marker
462 *OSR1* was expressed at higher level in *KO* cells comparing to the *WT* cells.

We then inspected RNA-seq data from *WT* and *KO* organoids at day 25 for the expression of LPM genes and markers of LPM derivatives. The expression of several LPM genes (*OSR1*, *FOXF1*, *FOXF2*, *FENDRR*, *HAND1*, *HAND2* and *CXCL12*) was strongly up-regulated in *KO* cells compared to *WT* cells suggesting that an LPM-like cell pool persisted in D25 *KO* organoids **(Figure 6A-I).** To further substantiate the potential differentiation of the *CEP83*-mutant cells into broadly LPM-like cells, we compared genes that were upregulated genes in D25 organoids (in total, 397 genes) with LPM genes that were previously identified by single cell transcriptomics of sorted post-gastrulation LPM cells from developing zebrafish[33,59,60]. Our targeted comparison documented that *CEP83*$^{-/-}$ organoids showed significant enrichment for expression of orthologs of early LPM genes (p=0.006) (**Figure 6- figure supplement 2)**, including *OSR1*, *CXCL12*, *HAND1/2*, *KCTD12*, *PIK3R3*, and *ZBTB2*. A subset of LPM genes enriched for expression in *CEP83*-mutant cells at D25 of differentiation were indicative of cardiac or cardiopharyngeal (*ISL1*, *TBX1*) as well as of vascular progenitor (*SOX7*, *SOX11*, *NAP1L3*, *LMO2*, *GATA2*) differentiation[70-77] (**Figure 6 J-P**). Taken together, these observations document that hiPSCs without *CEP83* respond to an *in vitro* differentiation program towards kidney progenitors, yet diverge towards a broader LPM progenitor composition without significant IM instead.

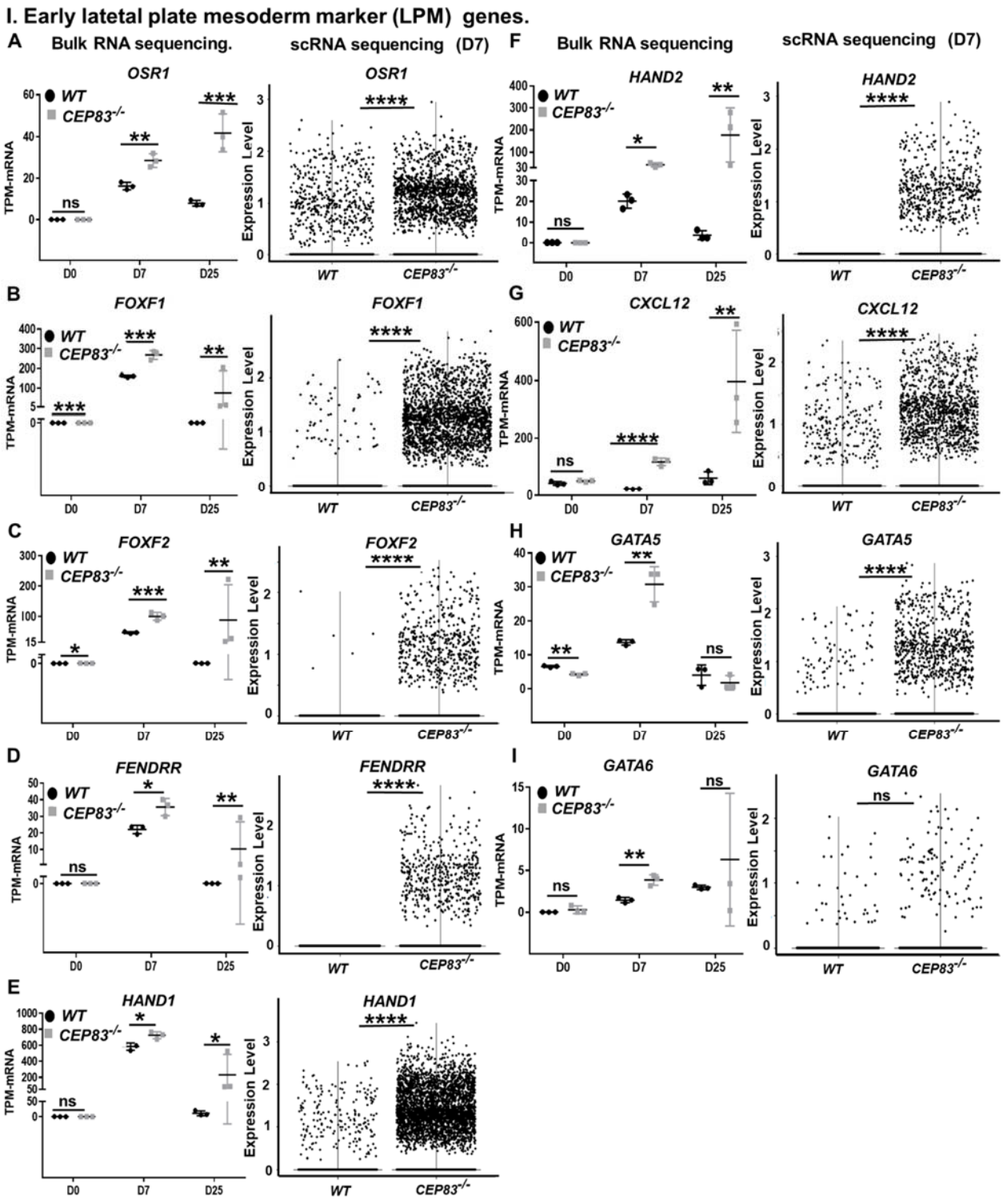

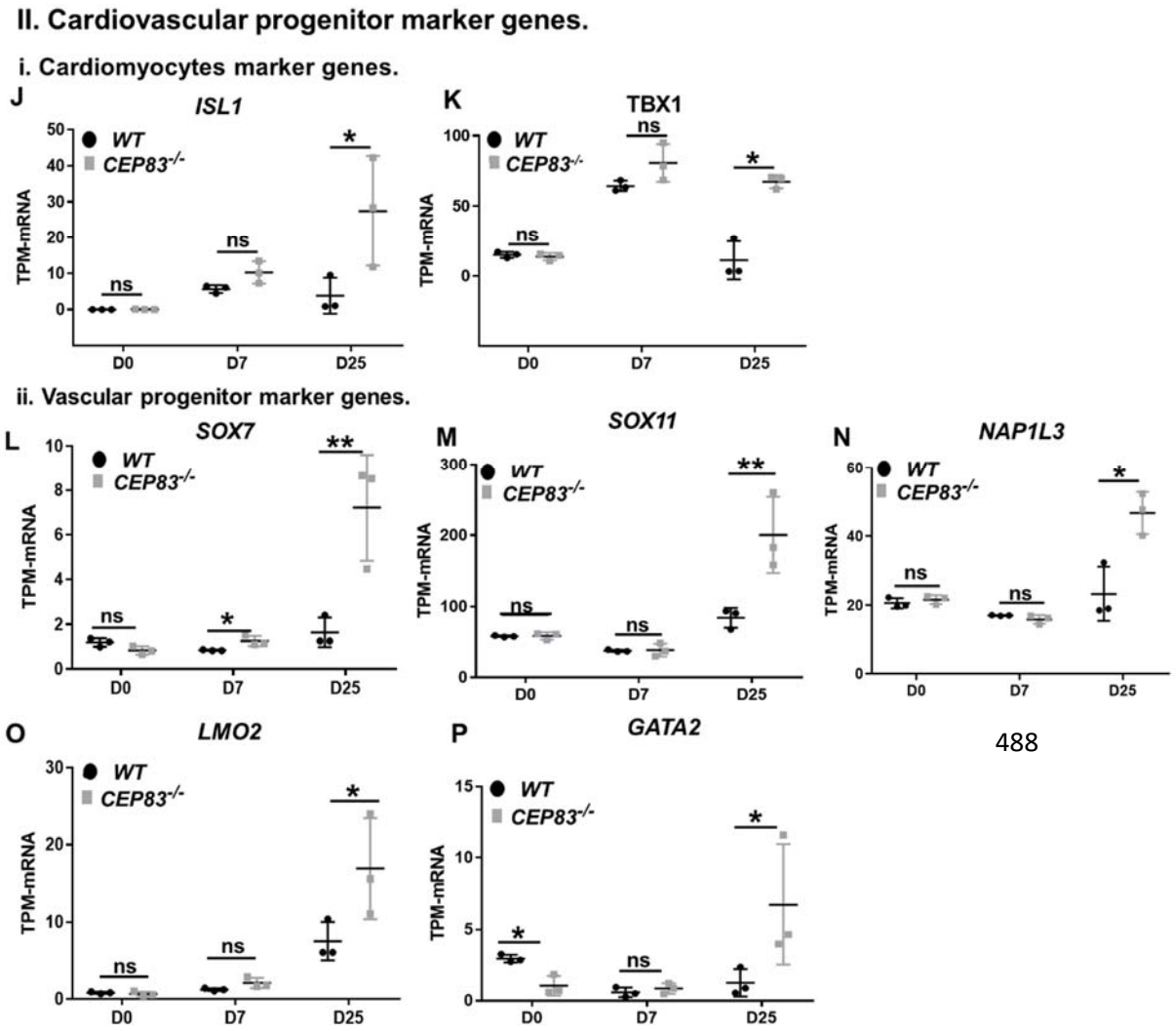

488

493 **Figure 6: *CEP83*$^{-/-}$ cells upregulate expression of genes characteristic of early lateral plate**
494 **mesoderm, cardiomyocyte progenitors and vascular progenitors. (A-I)** Expression of early lateral
495 plate mesoderm (LPM) markers *OSR1* (A), *FOXF1* (B), *FOXF2 (*C), *FENDRR* (D), *HAND1* (E), *HAND2* (F),
496 *CXCL12* (G), *GATA5* (H), and *GATA6* (I) in wildtype (*WT*) and *CEP83*$^{-/-}$ cells at day 0 (D0), day 7 (D7) and
497 day 25 (D25) according to bulk RNA-sequencing (left panels) and at D7 according to single cell RNA
498 sequencing (right panels). (J-P) Expression of cardiomyocyte markers *ISL1* (J), *TBX1* (K) and vascular
499 progenitor markers *SOX7* (L), *SOX11* (M), *NAP1L3* (N), *LMO2* (O) and *GATA2* (P) in wildtype (*WT*) and
500 *CEP83*$^{-/-}$ cells at day 0 (D0), day 7 (D7) and day 25 (D25) according to bulk RNA-sequencing. N = 3 clones
501 per group for bulk RNA seq. N = 2 clones per group for scRNA-seq. Expression units are mean transcripts
502 per million (TPM) ± SD. *P < 0.05, **P < 0.01, ***P < 0.001 and ****P < 0.0001. ns= not significant. See

Figure 6- figure supplements 1- 2. See also Figure 6- source data 1. Check data availability section for other source data.

Discussion:

This study indicates a novel contribution of CEP83 in regulating the differentiation path from human pluripotent stem cells to kidney progenitors. We pinpoint a stage at day 7 of intermediate mesoderm induction where *CEP83* loss of function results in a decreased nephron progenitor pool with down-regulation of critical kidney progenitor genes (*PAX8*, *EYA1*, *HOXB7*). At the same stage, genes typical of LPM specification (including *FOXF1, FOXF2, FENDRR, HAND1, HAND2*) are up-regulated **(Figure 7)**. Functionally, these alterations are associated with an inability of *CEP83*-deficient cells to form kidney epithelia. Organoids derived from *CEP83*-deficient cells fail to induce any detectable nephron structures, suggesting a novel role for CEP83 during the specification of functional kidney progenitors in the mesoderm.

Our findings are relevant to understanding cellular and molecular functions of CEP83 and might be relevant to the pathophysiology of human genetic diseases. To date, eleven patients with biallelic mutations of *CEP83* have been reported, eight of which displayed kidney phenotypes[9,78,79]. Available kidney histologies identified microcystic tubular dilatations, tubular atrophy, thickened basement membranes and interstitial fibrosis. Extrarenal phenotypes included speech delay, intellectual disability, hydrocephalus, strabismus, retinal degeneration, retinitis pigmentosa, hepatic cytolysis, cholestasis, and portal septal fibrosis with mild thickening of arterial walls and increase in the number of the biliary canalicules on liver biopsy. Among individuals with *CEP83* mutations, all but

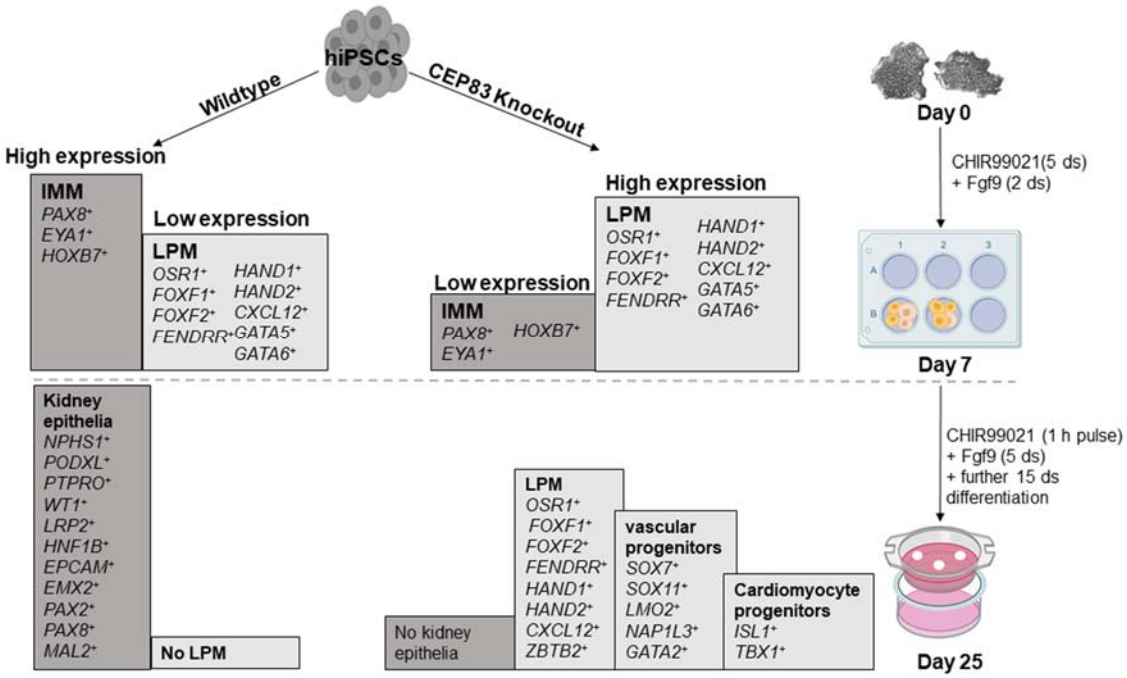

525 **Figure 7: Schematic model outlining the functional differences between wildtype and CEP83**
526 **knockout cells during the course of differentiation of human pluripotent stem cells towards kidney**
527 **cells.** Intermediate mesoderm, IMM; lateral plate mesoderm, LPM.

528 one carried at least one missense mutation or short in-frame deletion, suggesting that
529 *CEP83* function may have been partially preserved. One individual with presumed full
530 loss of *CEP83* displayed a more severe phenotype with multiple organ dysfunction. It will
531 be interesting to await future reports of additional *CEP83* mutations in humans and
532 whether complete loss of function alleles will result in broader mesoderm defects or renal
533 agenesis. In this regard, it is interesting that mice with a targeted homozygous loss-of-
534 function mutation of their *CEP83* ortholog (*Cep83*$^{tm1.1(KOMP)Vlcg}$) display midembryonic
535 lethality (at E12.5) with evidence of severe developmental delay as early as E9.5
536 (https://www.mousephenotype.org/data/genes/MGI:1924298). These phenotypes are
537 potentially consistent with a role of *CEP83* in germ layer patterning and mesoderm

development, but a more detailed phenotypical characterization of *Cep83* knockout embryos would be required to substantiate this possibility.

The precise molecular and cellular mechanisms underlying our observations remain to be determined. CEP83 is a protein that is necessary for the assembly of DAPs and primary cilia formation in several cell types[4,5,10,80-82]. A potential involvement of CEP83-mediated primary cilia formation in the findings reported here is suggested by obvious ciliary defects in CEP83-deficient cells at the D7 and at the organoid stage **(Figure 2D-G, Figure 2- figure supplement 1)**. These defects include reduced percentages of ciliated cells and elongated primary cilia in those cells that continue to form a primary cilium.

We observed downregulated expression of the key nephron progenitor genes *PAX8*, *EYA1,* and *HOXB7* in *CEP83*$^{-/-}$ cells at day 7, which might explain their failure to differentiate into kidney cells, since each of these genes is essential for normal kidney development [42,83-86]. Defects during nephron progenitor differentiation in the IM would be expected to result in severe kidney phenotypes such as renal agenesis or renal hypodysplasia. Defects of centriolar components or cilia have previously been linked to such phenotypes: in mice, centrosome amplification, i. e. the formation of excess centrosomes per cell, severely disrupts kidney development, resulting in depletion of renal progenitors and renal hypoplasia[87]. In humans, loss of KIF14, a protein necessary for proper DAP assembly and cilium formation, has been associated with kidney malformations, including renal agenesis and renal dysplasia[88-90]. Furthermore, Kif3a, a ciliary protein involved in intraflagellar transport, is necessary for normal mesoderm formation and kidney progenitor-specific defects of Kif3a have been associated with

561 reduced nephron numbers[91,92]. Similarly, mouse genes encoding the ciliary intraflagellar
562 transport proteins IFT25 and IFT27 have been associated with renal agenesis or renal
563 hypoplasia[93,94]. Together, these studies highlight the importance of molecules involved in
564 ciliogenesis for mesoderm and kidney progenitor development and suggest that CEP83
565 contributes to such processes by facilitating an early step of ciliogenesis. Nevertheless,
566 the detailed molecular processes that link CEP83 function, cilia formation, and kidney
567 progenitor specification remain to be determined.

568 The finding of various upregulated LPM markers in *CEP83*$^{-/-}$ cells starting from day 7
569 suggests that CEP83 function maybe involved in finetuning the balance of LPM and IM,
570 thereby contributing to lineage decisions during mesoderm formation. Crosstalk of LPM
571 and IM has been reported previously in zebrafish, overexpression of LPM transcription
572 factors Scl/Tal1 and Lmo2 induces ectopic vessel and blood specification while inhibiting
573 IM formation[95]. Furthermore, the LPM transcription factor Hand2 is critical in determining
574 the size of the IM, while natively expressed in the IM-adjacent LPM progenitors that form
575 mesothelia[33,58]. Loss of Hand2 in zebrafish results in an expanded IM, whereas Hand2
576 overexpression reduces or abolishes the IM. Interestingly, HAND2 was among the most
577 strongly induced transcripts in our *CEP83*$^{-/-}$ cells at day 7; connecting with the
578 developmental role of Hand2 in IM formation, these observations suggest that HAND2
579 expression in CEP83-deficient cells may have contributed to the reduced numbers of
580 nephron progenitor cells at this stage. Of note, CEP83-deficient cells at D25 expressed
581 increased levels of LPM genes expressed in mesothelial (including *OSR1*, *CXCL12*,
582 *HAND1/2*), cardiopharyngeal (including *ISL1*, *TBX1*), and endothelial/hematopoietic
583 (including *TAL1*, *LMO2*, *GATA2*) progenitors[33,60]. In sum, we propose a novel role for

584 CEP83 in regulating the development of IM nephron progenitors, which may involve direct
585 effects of CEP83 in the nephron progenitor differentiation program and indirect LPM-
586 mediated effects on the IM. Future studies are warranted to delineate the molecular and
587 cellular mechanisms underlying CEP83 function in LPM and specifically IM patterning.

588 **Acknowledgements:**

589 We thank Tatjana Luganskaja for excellent technical support. This work was supported
590 by grants to K.M.S.-O. from the Deutsche Forschungsgemeinschaft (DFG; SFB 1365,
591 GRK 2318 and FOR 2841), by stipends to F.M. by the Egyptian government, by the
592 Urological Research Foundation (Berlin), a Swiss National Science Foundation
593 postdoctoral fellowship to J.K.-R., and the University of Colorado School of Medicine,
594 Anschutz Medical Campus, and the Children's Hospital Colorado Foundation to C.M..

595 **Competing interests: none**

596

597 **Data availability**

598 All data supporting the findings of this study are available within the article and its
599 supplementary files. Source data files have been provided for Figures 1 to 6. Sequencing
600 data have been deposited in GEO at
601 https://www.ncbi.nlm.nih.gov/geo/query/acc.cgi?acc=GSE205978 (Reviewers TOKEN:
602 mzkfymcwzzwptib).

603

604

References:

1 Davidson, A. J., Lewis, P., Przepiorski, A. & Sander, V. Turning mesoderm into kidney. *Seminars in cell & developmental biology* **91**, 86-93, doi:10.1016/j.semcdb.2018.08.016 (2019).

2 Prummel, K. D., Nieuwenhuize, S. & Mosimann, C. The lateral plate mesoderm. *Development (Cambridge, England)* **147**, doi:10.1242/dev.175059 (2020).

3 Lo, C.-H., Lin, I., Yang, T. T., Huang, Y.-C., Tanos, B. E., Chou, P.-C., Chang, C.-W., Tsay, Y.-G., Liao, J.-C. & Wang, W.-J. Phosphorylation of CEP83 by TTBK2 is necessary for cilia initiation. *Journal of Cell Biology* **218**, 3489-3505 (2019).

4 Tanos, B. E., Yang, H.-J., Soni, R., Wang, W.-J., Macaluso, F. P., Asara, J. M. & Tsou, M.-F. B. Centriole distal appendages promote membrane docking, leading to cilia initiation. *Genes & development* **27**, 163-168 (2013).

5 Yang, T. T., Chong, W. M., Wang, W.-J., Mazo, G., Tanos, B., Chen, Z., Tran, T. M. N., Chen, Y.-D., Weng, R. R. & Huang, C.-E. Super-resolution architecture of mammalian centriole distal appendages reveals distinct blade and matrix functional components. *Nature communications* **9**, 1-11 (2018).

6 Kurtulmus, B., Yuan, C., Schuy, J., Neuner, A., Hata, S., Kalamakis, G., Martin-Villalba, A. & Pereira, G. LRRC45 contributes to early steps of axoneme extension. *Journal of cell science* **131** (2018).

7 Wheway, G., Schmidts, M., Mans, D. A., Szymanska, K., Nguyen, T. T., Racher, H., Phelps, I. G., Toedt, G., Kennedy, J., Wunderlich, K. A., Sorusch, N., Abdelhamed, Z. A., Natarajan, S., Herridge, W., van Reeuwijk, J., Horn, N., Boldt, K., Parry, D. A., Letteboer, S. J. F., Roosing, S., Adams, M., Bell, S. M., Bond, J., Higgins, J., Morrison, E. E., Tomlinson, D. C., Slaats, G. G., van Dam, T. J. P., Huang, L., Kessler, K., Giessl, A., Logan, C. V., Boyle, E. A., Shendure, J., Anazi, S., Aldahmesh, M., Al Hazzaa, S., Hegele, R. A., Ober, C., Frosk, P., Mhanni, A. A., Chodirker, B. N., Chudley, A. E., Lamont, R., Bernier, F. P., Beaulieu, C. L., Gordon, P., Pon, R. T., Donahue, C., Barkovich, A. J., Wolf, L., Toomes, C., Thiel, C. T., Boycott, K. M., McKibbin, M., Inglehearn, C. F., Stewart, F., Omran, H., Huynen, M. A., Sergouniotis, P. I., Alkuraya, F. S., Parboosingh, J. S., Innes, A. M., Willoughby, C. E., Giles, R. H., Webster, A. R., Ueffing, M., Blacque, O., Gleeson, J. G., Wolfrum, U., Beales, P. L., Gibson, T., Doherty, D., Mitchison, H. M., Roepman, R. & Johnson, C. A. An siRNA-based functional genomics screen for the identification of regulators of ciliogenesis and ciliopathy genes. *Nat Cell Biol* **17**, 1074-1087, doi:10.1038/ncb3201 (2015).

8 Bowler, M., Kong, D., Sun, S., Nanjundappa, R., Evans, L., Farmer, V., Holland, A., Mahjoub, M. R., Sui, H. & Loncarek, J. High-resolution characterization of centriole distal appendage morphology and dynamics by correlative STORM and electron microscopy. *Nature Communications* **10**, 993, doi:10.1038/s41467-018-08216-4 (2019).

9 Failler, M., Gee, H. Y., Krug, P., Joo, K., Halbritter, J., Belkacem, L., Filhol, E., Porath, J. D., Braun, D. A. & Schueler, M. Mutations of CEP83 cause infantile

649 nephronophthisis and intellectual disability. *The American Journal of Human*
650 *Genetics* **94**, 905-914 (2014).
651 10 Shao, W., Yang, J., He, M., Yu, X.-Y., Lee, C. H., Yang, Z., Joyner, A. L., Anderson,
652 K. V., Zhang, J. & Tsou, M.-F. B. Centrosome anchoring regulates progenitor
653 properties and cortical formation. *Nature* **580**, 106-112 (2020).
654 11 Mansour, F., Boivin, F. J., Shaheed, I. B., Schueler, M. & Schmidt-Ott, K. M. The
655 Role of Centrosome Distal Appendage Proteins (DAPs) in Nephronophthisis and
656 Ciliogenesis. *International journal of molecular sciences* **22**,
657 doi:10.3390/ijms222212253 (2021).
658 12 Hildebrandt, F. in *Pediatric Nephrology* (2004).
659 13 Luo, F. & Tao, Y. H. Nephronophthisis: a review of genotype–phenotype
660 correlation. *Nephrology* **23**, 904-911 (2018).
661 14 Takahashi, K., Tanabe, K., Ohnuki, M., Narita, M., Ichisaka, T., Tomoda, K. &
662 Yamanaka, S. Induction of pluripotent stem cells from adult human fibroblasts by
663 defined factors. *cell* **131**, 861-872 (2007).
664 15 Morizane, R., Lam, A. Q., Freedman, B. S., Kishi, S., Valerius, M. T. & Bonventre,
665 J. V. Nephron organoids derived from human pluripotent stem cells model kidney
666 development and injury. *Nature biotechnology* **33**, 1193-1200 (2015).
667 16 Taguchi, A., Kaku, Y., Ohmori, T., Sharmin, S., Ogawa, M., Sasaki, H. &
668 Nishinakamura, R. Redefining the in vivo origin of metanephric nephron
669 progenitors enables generation of complex kidney structures from pluripotent stem
670 cells. *Cell stem cell* **14**, 53-67 (2014).

17 Takasato, M., Er, P. X., Chiu, H. S., Maier, B., Baillie, G. J., Ferguson, C., Parton, R. G., Wolvetang, E. J., Roost, M. S., Chuva de Sousa Lopes, S. M. & Little, M. H. Kidney organoids from human iPS cells contain multiple lineages and model human nephrogenesis. *Nature* **526**, 564-568, doi:10.1038/nature15695 (2015).

18 Freedman, B. S., Brooks, C. R., Lam, A. Q., Fu, H., Morizane, R., Agrawal, V., Saad, A. F., Li, M. K., Hughes, M. R. & Vander Werff, R. Modelling kidney disease with CRISPR-mutant kidney organoids derived from human pluripotent epiblast spheroids. *Nature communications* **6**, 8715 (2015).

19 Kumar, S. V., Er, P. X., Lawlor, K. T., Motazedian, A., Scurr, M., Ghobrial, I., Combes, A. N., Zappia, L., Oshlack, A., Stanley, E. G. & Little, M. H. Kidney micro-organoids in suspension culture as a scalable source of human pluripotent stem cell-derived kidney cells. *Development (Cambridge, England)* **146**, dev172361, doi:10.1242/dev.172361 (2019).

20 Tan, Z., Shan, J., Rak-Raszewska, A. & Vainio, S. J. Embryonic stem cells derived kidney organoids as faithful models to target programmed nephrogenesis. *Scientific reports* **8**, 1-10 (2018).

21 Boyle, S., Misfeldt, A., Chandler, K. J., Deal, K. K., Southard-Smith, E. M., Mortlock, D. P., Baldwin, H. S. & de Caestecker, M. Fate mapping using Cited1-CreERT2 mice demonstrates that the cap mesenchyme contains self-renewing progenitor cells and gives rise exclusively to nephronic epithelia. *Developmental biology* **313**, 234-245 (2008).

22 Kobayashi, A., Valerius, M. T., Mugford, J. W., Carroll, T. J., Self, M., Oliver, G. & McMahon, A. P. Six2 defines and regulates a multipotent self-renewing nephron

progenitor population throughout mammalian kidney development. *Cell stem cell* **3**, 169-181 (2008).

23 Howden, S. E., Vanslambrouck, J. M., Wilson, S. B., Tan, K. S. & Little, M. H. Reporter-based fate mapping in human kidney organoids confirms nephron lineage relationships and reveals synchronous nephron formation. *EMBO reports* **20**, e47483 (2019).

24 Kuraoka, S., Tanigawa, S., Taguchi, A., Hotta, A., Nakazato, H., Osafune, K., Kobayashi, A. & Nishinakamura, R. PKD1-Dependent Renal Cystogenesis in Human Induced Pluripotent Stem Cell-Derived Ureteric Bud/Collecting Duct Organoids. *Journal of the American Society of Nephrology* **31**, 2355-2371 (2020).

25 Concordet, J.-P. & Haeussler, M. CRISPOR: intuitive guide selection for CRISPR/Cas9 genome editing experiments and screens. *Nucleic Acids Research* **46**, W242-W245, doi:10.1093/nar/gky354 (2018).

26 Yumlu, S., Stumm, J., Bashir, S., Dreyer, A.-K., Lisowski, P., Danner, E. & Kühn, R. Gene editing and clonal isolation of human induced pluripotent stem cells using CRISPR/Cas9. *Methods* **121-122**, 29-44, doi:https://doi.org/10.1016/j.ymeth.2017.05.009 (2017).

27 LaFramboise, T. Single nucleotide polymorphism arrays: a decade of biological, computational and technological advances. *Nucleic Acids Research* **37**, 4181-4193, doi:10.1093/nar/gkp552 (2009).

28 Arsham, M. S., Barch, M. J. & Lawce, H. J. *The AGT cytogenetics laboratory manual*. (John Wiley & Sons, 2017).

716 29 Haraksingh, R. R., Abyzov, A. & Urban, A. E. Comprehensive performance
717 comparison of high-resolution array platforms for genome-wide Copy Number
718 Variation (CNV) analysis in humans. *BMC genomics* **18**, 1-14 (2017).
719 30 Robinson, J. T., Thorvaldsdóttir, H., Winckler, W., Guttman, M., Lander, E. S.,
720 Getz, G. & Mesirov, J. P. Integrative genomics viewer. *Nature biotechnology* **29**,
721 24-26 (2011).
722 31 Alles, J., Karaiskos, N., Praktiknjo, S. D., Grosswendt, S., Wahle, P., Ruffault, P.-
723 L., Ayoub, S., Schreyer, L., Boltengagen, A. & Birchmeier, C. Cell fixation and
724 preservation for droplet-based single-cell transcriptomics. *BMC biology* **15**, 1-14
725 (2017).
726 32 Stuart, T., Butler, A., Hoffman, P., Hafemeister, C., Papalexi, E., Mauck III, W. M.,
727 Hao, Y., Stoeckius, M., Smibert, P. & Satija, R. Comprehensive integration of
728 single-cell data. *Cell* **177**, 1888-1902. e1821 (2019).
729 33 Prummel, K. D., Crowell, H. L., Nieuwenhuize, S., Brombacher, E. C., Daetwyler,
730 S., Soneson, C., Kresoja-Rakic, J., Kocere, A., Ronner, M., Ernst, A., Labbaf, Z.,
731 Clouthier, D. E., Firulli, A. B., Sánchez-Iranzo, H., Naganathan, S. R., O'Rourke,
732 R., Raz, E., Mercader, N., Burger, A., Felley-Bosco, E., Huisken, J., Robinson, M.
733 D. & Mosimann, C. Hand2 delineates mesothelium progenitors and is reactivated
734 in mesothelioma. *Nature Communications* **13**, 1677, doi:10.1038/s41467-022-
735 29311-7 (2022).
736 34 Takasato, M., Pei, X. E., Chiu, H. S., Maier, B., Baillie, G. J., Ferguson, C., Parton,
737 R. G., Wolvetang, E. J., Roost, M. S. & de Sousa Lopes, S. M. C. Kidney organoids

from human iPS cells contain multiple lineages and model human nephrogenesis. *Nature* **526**, 564-568 (2015).

35 Bilous, R. W., Murty, G., Parkinson, D. B., Thakker, R. V., Coulthard, M. G., Burn, J., Mathias, D. & Kendall-Taylor, P. Autosomal dominant familial hypoparathyroidism, sensorineural deafness, and renal dysplasia. *New England Journal of Medicine* **327**, 1069-1074 (1992).

36 Grote, D., Souabni, A., Busslinger, M. & Bouchard, M. Pax2/8-regulated Gata3 expression is necessary for morphogenesis and guidance of the nephric duct in the developing kidney. *Development (Cambridge, England)* **133**, 53-61, doi:10.1242/dev.02184 (2006).

37 Kress, C., Vogels, R., De Graaff, W., Bonnerot, C., Meijlink, F., Nicolas, J.-F. & Deschamps, J. Hox-2.3 upstream sequences mediate lacZ expression in intermediate mesoderm derivatives of transgenic mice. *Development (Cambridge, England)* **109**, 775-786 (1990).

38 Srinivas, S., Wu, Z., Chen, C.-M., D'Agati, V. & Costantini, F. Dominant effects of RET receptor misexpression and ligand-independent RET signaling on ureteric bud development. *Development (Cambridge, England)* **126**, 1375-1386 (1999).

39 Wellik, D. M., Hawkes, P. J. & Capecchi, M. R. Hox11 paralogous genes are essential for metanephric kidney induction. *Genes & development* **16**, 1423-1432 (2002).

40 Mugford, J. W., Sipilä, P., Kobayashi, A., Behringer, R. R. & McMahon, A. P. Hoxd11 specifies a program of metanephric kidney development within the

intermediate mesoderm of the mouse embryo. *Developmental biology* **319**, 396-405, doi:10.1016/j.ydbio.2008.03.044 (2008).

41 Ruf, R. G., Xu, P.-X., Silvius, D., Otto, E. A., Beekmann, F., Muerb, U. T., Kumar, S., Neuhaus, T. J., Kemper, M. J. & Raymond, R. M. SIX1 mutations cause branchio-oto-renal syndrome by disruption of EYA1–SIX1–DNA complexes. *Proceedings of the National Academy of Sciences* **101**, 8090-8095 (2004).

42 Sajithlal, G., Zou, D., Silvius, D. & Xu, P.-X. Eya1 acts as a critical regulator for specifying the metanephric mesenchyme. *Developmental Biology* **284**, 323-336, doi:https://doi.org/10.1016/j.ydbio.2005.05.029 (2005).

43 Subramanian, A., Sidhom, E.-H., Emani, M., Vernon, K., Sahakian, N., Zhou, Y., Kost-Alimova, M., Slyper, M., Waldman, J., Dionne, D., Nguyen, L. T., Weins, A., Marshall, J. L., Rosenblatt-Rosen, O., Regev, A. & Greka, A. Single cell census of human kidney organoids shows reproducibility and diminished off-target cells after transplantation. *Nature Communications* **10**, 5462, doi:10.1038/s41467-019-13382-0 (2019).

44 Low, J. H., Li, P., Chew, E. G. Y., Zhou, B., Suzuki, K., Zhang, T., Lian, M. M., Liu, M., Aizawa, E. & Esteban, C. R. Generation of human PSC-derived kidney organoids with patterned nephron segments and a de novo vascular network. *Cell Stem Cell* **25**, 373-387. e379 (2019).

45 Mugford, J. W., Sipilä, P., McMahon, J. A. & McMahon, A. P. Osr1 expression demarcates a multi-potent population of intermediate mesoderm that undergoes progressive restriction to an Osr1-dependent nephron progenitor compartment within the mammalian kidney. *Developmental biology* **324**, 88-98 (2008).

783 46 Mae, S.-I., Shono, A., Shiota, F., Yasuno, T., Kajiwara, M., Gotoda-Nishimura, N.,
784 Arai, S., Sato-Otubo, A., Toyoda, T., Takahashi, K., Nakayama, N., Cowan, C. A.,
785 Aoi, T., Ogawa, S., McMahon, A. P., Yamanaka, S. & Osafune, K. Monitoring and
786 robust induction of nephrogenic intermediate mesoderm from human pluripotent
787 stem cells. *Nature Communications* **4**, 1367, doi:10.1038/ncomms2378 (2013).
788 47 Mahlapuu, M., Ormestad, M., Enerbäck, S. & Carlsson, P. The forkhead
789 transcription factor Foxf1 is required for differentiation of extra-embryonic and
790 lateral plate mesoderm. *Development (Cambridge, England)* **128**, 155-166 (2001).
791 48 Ormestad, M., Astorga, J. & Carlsson, P. Differences in the embryonic expression
792 patterns of mouse Foxf1 and -2 match their distinct mutant phenotypes. *Dev Dyn*
793 **229**, 328-333, doi:10.1002/dvdy.10426 (2004).
794 49 Wilm, B., James, R. G., Schultheiss, T. M. & Hogan, B. L. M. The forkhead genes,
795 Foxc1 and Foxc2, regulate paraxial versus intermediate mesoderm cell fate.
796 *Developmental Biology* **271**, 176-189,
797 doi:https://doi.org/10.1016/j.ydbio.2004.03.034 (2004).
798 50 Wotton, K. R., Mazet, F. & Shimeld, S. M. Expression of FoxC, FoxF, FoxL1, and
799 FoxQ1 genes in the dogfish Scyliorhinus canicula defines ancient and derived
800 roles for Fox genes in vertebrate development. *Developmental dynamics: an*
801 *official publication of the American Association of Anatomists* **237**, 1590-1603
802 (2008).
803 51 Grote, P., Wittler, L., Hendrix, D., Koch, F., Währisch, S., Beisaw, A., Macura, K.,
804 Bläss, G., Kellis, M. & Werber, M. The tissue-specific lncRNA Fendrr is an essential

regulator of heart and body wall development in the mouse. *Developmental cell* **24**, 206-214 (2013).

52 Schindler, Y. L., Garske, K. M., Wang, J., Firulli, B. A., Firulli, A. B., Poss, K. D. & Yelon, D. Hand2 elevates cardiomyocyte production during zebrafish heart development and regeneration. *Development (Cambridge, England)* **141**, 3112-3122, doi:10.1242/dev.106336 (2014).

53 Tsuchihashi, T., Maeda, J., Shin, C. H., Ivey, K. N., Black, B. L., Olson, E. N., Yamagishi, H. & Srivastava, D. Hand2 function in second heart field progenitors is essential for cardiogenesis. *Developmental biology* **351**, 62-69, doi:10.1016/j.ydbio.2010.12.023 (2011).

54 McFadden, D. G., Barbosa, A. C., Richardson, J. A., Schneider, M. D., Srivastava, D. & Olson, E. N. The Hand1 and Hand2 transcription factors regulate expansion of the embryonic cardiac ventricles in a gene dosage-dependent manner. (2005).

55 Firulli, A. B., McFadden, D. G., Lin, Q., Srivastava, D. & Olson, E. N. Heart and extra-embryonic mesodermal defects in mouse embryos lacking the bHLH transcription factor Hand1. *Nature genetics* **18**, 266-270 (1998).

56 Risebro, C. A., Smart, N., Dupays, L., Breckenridge, R., Mohun, T. J. & Riley, P. R. Hand1 regulates cardiomyocyte proliferation versus differentiation in the developing heart. *Development (Cambridge, England)* **133**, 4595-4606, doi:10.1242/dev.02625 (2006).

57 Angelo, S., Lohr, J., Lee, K. H., Ticho, B. S., Breitbart, R. E., Hill, S., Yost, H. J. & Srivastava, D. Conservation of sequence and expression of Xenopus and

827 zebrafish dHAND during cardiac, branchial arch and lateral mesoderm
828 development. *Mechanisms of development* **95**, 231-237 (2000).
829 58 Perens, E. A., Garavito-Aguilar, Z. V., Guio-Vega, G. P., Peña, K. T., Schindler, Y.
830 L. & Yelon, D. Hand2 Inhibits Kidney Specification While Promoting Vein
831 Formation Within the Posterior Mesoderm. *bioRxiv*, 075036, doi:10.1101/075036
832 (2016).
833 59 Prummel, K. D., Crowell, H. L., Nieuwenhuize, S., Brombacher, E. C., Daetwyler,
834 S., Soneson, C., Kresoja-Rakic, J., Ronner, M., Kocere, A. & Ernst, A. Hand2
835 delineates mesothelium progenitors and is reactivated in mesothelioma. *bioRxiv*,
836 2020.2011. 2011.355693 (2021).
837 60 Prummel, K. D., Nieuwenhuize, S. & Mosimann, C. The lateral plate mesoderm.
838 *Development (Cambridge, England)* **147**, dev175059 (2020).
839 61 Salcedo, R. & Oppenheim, J. J. Role of chemokines in angiogenesis:
840 CXCL12/SDF-1 and CXCR4 interaction, a key regulator of endothelial cell
841 responses. *Microcirculation* **10**, 359-370 (2003).
842 62 Liekens, S., Schols, D. & Hatse, S. CXCL12-CXCR4 axis in angiogenesis,
843 metastasis and stem cell mobilization. *Current pharmaceutical design* **16**, 3903-
844 3920 (2010).
845 63 Loh, K. M., Chen, A., Koh, P. W., Deng, T. Z., Sinha, R., Tsai, J. M., Barkal, A. A.,
846 Shen, K. Y., Jain, R., Morganti, R. M., Shyh-Chang, N., Fernhoff, N. B., George,
847 B. M., Wernig, G., Salomon, R. E. A., Chen, Z., Vogel, H., Epstein, J. A., Kundaje,
848 A., Talbot, W. S., Beachy, P. A., Ang, L. T. & Weissman, I. L. Mapping the Pairwise

Choices Leading from Pluripotency to Human Bone, Heart, and Other Mesoderm Cell Types. *Cell* **166**, 451-467, doi:10.1016/j.cell.2016.06.011 (2016).

64 Koutsourakis, M., Langeveld, A., Patient, R., Beddington, R. & Grosveld, F. The transcription factor GATA6 is essential for early extraembryonic development. *Development (Cambridge, England)* **126**, 723-732 (1999).

65 Holtzinger, A. & Evans, T. Gata5 and Gata6 are functionally redundant in zebrafish for specification of cardiomyocytes. *Developmental biology* **312**, 613-622 (2007).

66 Reiter, J. F., Alexander, J., Rodaway, A., Yelon, D., Patient, R., Holder, N. & Stainier, D. Y. Gata5 is required for the development of the heart and endoderm in zebrafish. *Genes & development* **13**, 2983-2995 (1999).

67 Pikkarainen, S., Tokola, H., Kerkelä, R. & Ruskoaho, H. GATA transcription factors in the developing and adult heart. *Cardiovascular research* **63**, 196-207 (2004).

68 Laverriere, A. C., MacNeill, C., Mueller, C., Poelmann, R. E., Burch, J. & Evans, T. GATA-4/5/6, a subfamily of three transcription factors transcribed in developing heart and gut. *Journal of Biological Chemistry* **269**, 23177-23184 (1994).

69 Zhao, R., Watt, A. J., Battle, M. A., Li, J., Bondow, B. J. & Duncan, S. A. Loss of both GATA4 and GATA6 blocks cardiac myocyte differentiation and results in acardia in mice. *Developmental Biology* **317**, 614-619, doi:https://doi.org/10.1016/j.ydbio.2008.03.013 (2008).

70 Cai, C.-L., Liang, X., Shi, Y., Chu, P.-H., Pfaff, S. L., Chen, J. & Evans, S. Isl1 identifies a cardiac progenitor population that proliferates prior to differentiation and contributes a majority of cells to the heart. *Developmental cell* **5**, 877-889 (2003).

872 71 Kwon, C., Qian, L., Cheng, P., Nigam, V., Arnold, J. & Srivastava, D. A regulatory
873 pathway involving Notch1/β-catenin/Isl1 determines cardiac progenitor cell fate.
874 *Nature cell biology* **11**, 951-957 (2009).
875 72 Laugwitz, K.-L., Moretti, A., Lam, J., Gruber, P., Chen, Y., Woodard, S., Lin, L.-Z.,
876 Cai, C.-L., Lu, M. M. & Reth, M. Postnatal isl1+ cardioblasts enter fully
877 differentiated cardiomyocyte lineages. *Nature* **433**, 647-653 (2005).
878 73 Moretti, A., Caron, L., Nakano, A., Lam, J. T., Bernshausen, A., Chen, Y., Qyang,
879 Y., Bu, L., Sasaki, M. & Martin-Puig, S. Multipotent embryonic isl1+ progenitor cells
880 lead to cardiac, smooth muscle, and endothelial cell diversification. *Cell* **127**, 1151-
881 1165 (2006).
882 74 Gao, R., Liang, X., Cheedipudi, S., Cordero, J., Jiang, X., Zhang, Q., Caputo, L.,
883 Günther, S., Kuenne, C., Ren, Y., Bhattacharya, S., Yuan, X., Barreto, G., Chen,
884 Y., Braun, T., Evans, S. M., Sun, Y. & Dobreva, G. Pioneering function of Isl1 in
885 the epigenetic control of cardiomyocyte cell fate. *Cell Research* **29**, 486-501,
886 doi:10.1038/s41422-019-0168-1 (2019).
887 75 Stennard, F. A. & Harvey, R. P. T-box transcription factors and their roles in
888 regulatory hierarchies in the developing heart. *Development (Cambridge, England)*
889 **132**, 4897-4910, doi:10.1242/dev.02099 (2005).
890 76 Baldini, A. Dissecting contiguous gene defects: TBX1. *Current opinion in genetics*
891 *& development* **15**, 279-284, doi:10.1016/j.gde.2005.03.001 (2005).
892 77 Chen, L., Fulcoli, F. G., Tang, S. & Baldini, A. Tbx1 regulates proliferation and
893 differentiation of multipotent heart progenitors. *Circ Res* **105**, 842-851,
894 doi:10.1161/CIRCRESAHA.109.200295 (2009).

78 Veldman, B. C. F., Kuper, W. F. E., Lilien, M., Schuurs-Hoeijmakers, J. H. M., Marcelis, C., Phan, M., Hettinga, Y., Talsma, H. E., van Hasselt, P. M. & Haijes, H. A. Beyond nephronophthisis: Retinal dystrophy in the absence of kidney dysfunction in childhood expands the clinical spectrum of CEP83 deficiency. *American journal of medical genetics. Part A* **185**, 2204-2210, doi:10.1002/ajmg.a.62225 (2021).

79 Haer-Wigman, L., van Zelst-Stams, W. A. G., Pfundt, R., van den Born, L. I., Klaver, C. C. W., Verheij, J. B. G. M., Hoyng, C. B., Breuning, M. H., Boon, C. J. F., Kievit, A. J., Verhoeven, V. J. M., Pott, J. W. R., Sallevelt, S. C. E. H., van Hagen, J. M., Plomp, A. S., Kroes, H. Y., Lelieveld, S. H., Hehir-Kwa, J. Y., Castelein, S., Nelen, M., Scheffer, H., Lugtenberg, D., Cremers, F. P. M., Hoefsloot, L. & Yntema, H. G. Diagnostic exome sequencing in 266 Dutch patients with visual impairment. *European Journal of Human Genetics* **25**, 591-599, doi:10.1038/ejhg.2017.9 (2017).

80 Kumar, D., Rains, A., Herranz-Pérez, V., Lu, Q., Shi, X., Swaney, D. L., Stevenson, E., Krogan, N. J., Huang, B., Westlake, C., Garcia-Verdugo, J. M., Yoder, B. K. & Reiter, J. F. A ciliopathy complex builds distal appendages to initiate ciliogenesis. *The Journal of cell biology* **220**, doi:10.1083/jcb.202011133 (2021).

81 Stinchcombe, J. C., Randzavola, L. O., Angus, K. L., Mantell, J. M., Verkade, P. & Griffiths, G. M. Mother Centriole Distal Appendages Mediate Centrosome Docking at the Immunological Synapse and Reveal Mechanistic Parallels with Ciliogenesis. *Current biology : CB* **25**, 3239-3244, doi:10.1016/j.cub.2015.10.028 (2015).

917 82 Joo, K., Kim, C. G., Lee, M.-S., Moon, H.-Y., Lee, S.-H., Kim, M. J., Kweon, H.-S.,
918 Park, W.-Y., Kim, C.-H., Gleeson, J. G. & Kim, J. CCDC41 is required for ciliary
919 vesicle docking to the mother centriole. *Proceedings of the National Academy of*
920 *Sciences* **110**, 5987-5992, doi:10.1073/pnas.1220927110 (2013).
921 83 Bouchard, M., Souabni, A., Mandler, M., Neubüser, A. & Busslinger, M. Nephric
922 lineage specification by Pax2 and Pax8. *Genes & development* **16**, 2958-2970
923 (2002).
924 84 Xu, P.-X., Adams, J., Peters, H., Brown, M. C., Heaney, S. & Maas, R. Eya1-
925 deficient mice lack ears and kidneys and show abnormal apoptosis of organ
926 primordia. *Nature Genetics* **23**, 113-117, doi:10.1038/12722 (1999).
927 85 Patterson, L. T. & Potter, S. S. Atlas of Hox gene expression in the developing
928 kidney. *Developmental Dynamics* **229**, 771-779,
929 doi:https://doi.org/10.1002/dvdy.10474 (2004).
930 86 Rojek, A., Füchtbauer, E.-M., Kwon, T.-H., Frøkiær, J. & Nielsen, S. Severe urinary
931 concentrating defect in renal collecting duct-selective AQP2 conditional-knockout
932 mice. *Proceedings of the National Academy of Sciences* **103**, 6037-6042,
933 doi:10.1073/pnas.0511324103 (2006).
934 87 Dionne, L. K., Shim, K., Hoshi, M., Cheng, T., Wang, J., Marthiens, V., Knoten, A.,
935 Basto, R., Jain, S. & Mahjoub, M. R. Centrosome amplification disrupts renal
936 development and causes cystogenesis. *The Journal of cell biology* **217**, 2485-
937 2501, doi:10.1083/jcb.201710019 (2018).
938 88 Filges, I., Nosova, E., Bruder, E., Tercanli, S., Townsend, K., Gibson, W.,
939 Röthlisberger, B., Heinimann, K., Hall, J. & Gregory-Evans, C. Exome sequencing

identifies mutations in KIF14 as a novel cause of an autosomal recessive lethal fetal ciliopathy phenotype. *Clinical genetics* **86**, 220-228 (2014).

89 Reilly, M. L., Stokman, M. F., Magry, V., Jeanpierre, C., Alves, M., Paydar, M., Hellinga, J., Delous, M., Pouly, D. & Failler, M. Loss-of-function mutations in KIF14 cause severe microcephaly and kidney development defects in humans and zebrafish. *Human molecular genetics* **28**, 778-795 (2019).

90 Pejskova, P., Reilly, M. L., Bino, L., Bernatik, O., Dolanska, L., Ganji, R. S., Zdrahal, Z., Benmerah, A. & Cajanek, L. KIF14 controls ciliogenesis via regulation of Aurora A and is important for Hedgehog signaling. *The Journal of cell biology* **219**, doi:10.1083/jcb.201904107 (2020).

91 Takeda, S., Yonekawa, Y., Tanaka, Y., Okada, Y., Nonaka, S. & Hirokawa, N. Left-Right Asymmetry and Kinesin Superfamily Protein KIF3A: New Insights in Determination of Laterality and Mesoderm Induction by kif3A−/− Mice Analysis. *Journal of Cell Biology* **145**, 825-836, doi:10.1083/jcb.145.4.825 (1999).

92 Chi, L., Galtseva, A., Chen, L., Mo, R., Hui, C. C. & Rosenblum, N. D. Kif3a controls murine nephron number via GLI3 repressor, cell survival, and gene expression in a lineage-specific manner. *PloS one* **8**, e65448, doi:10.1371/journal.pone.0065448 (2013).

93 Desai, P. B., San Agustin, J. T., Stuck, M. W., Jonassen, J. A., Bates, C. M. & Pazour, G. J. Ift25 is not a cystic kidney disease gene but is required for early steps of kidney development. *Mechanisms of development* **151**, 10-17, doi:10.1016/j.mod.2018.04.001 (2018).

94 Quélin, C., Loget, P., Boutaud, L., Elkhartoufi, N., Milon, J., Odent, S., Fradin, M., Demurger, F., Pasquier, L., Thomas, S. & Attié-Bitach, T. Loss of function IFT27 variants associated with an unclassified lethal fetal ciliopathy with renal agenesis. *American journal of medical genetics. Part A* **176**, 1610-1613, doi:10.1002/ajmg.a.38685 (2018).

95 Gering, M., Yamada, Y., Rabbitts, T. H. & Patient, R. K. Lmo2 and Scl/Tal1 convert non-axial mesoderm into haemangioblasts which differentiate into endothelial cells in the absence of Gata1. *Development (Cambridge, England)* **130**, 6187-6199, doi:10.1242/dev.00875 (2003).

Supplemental Figures:

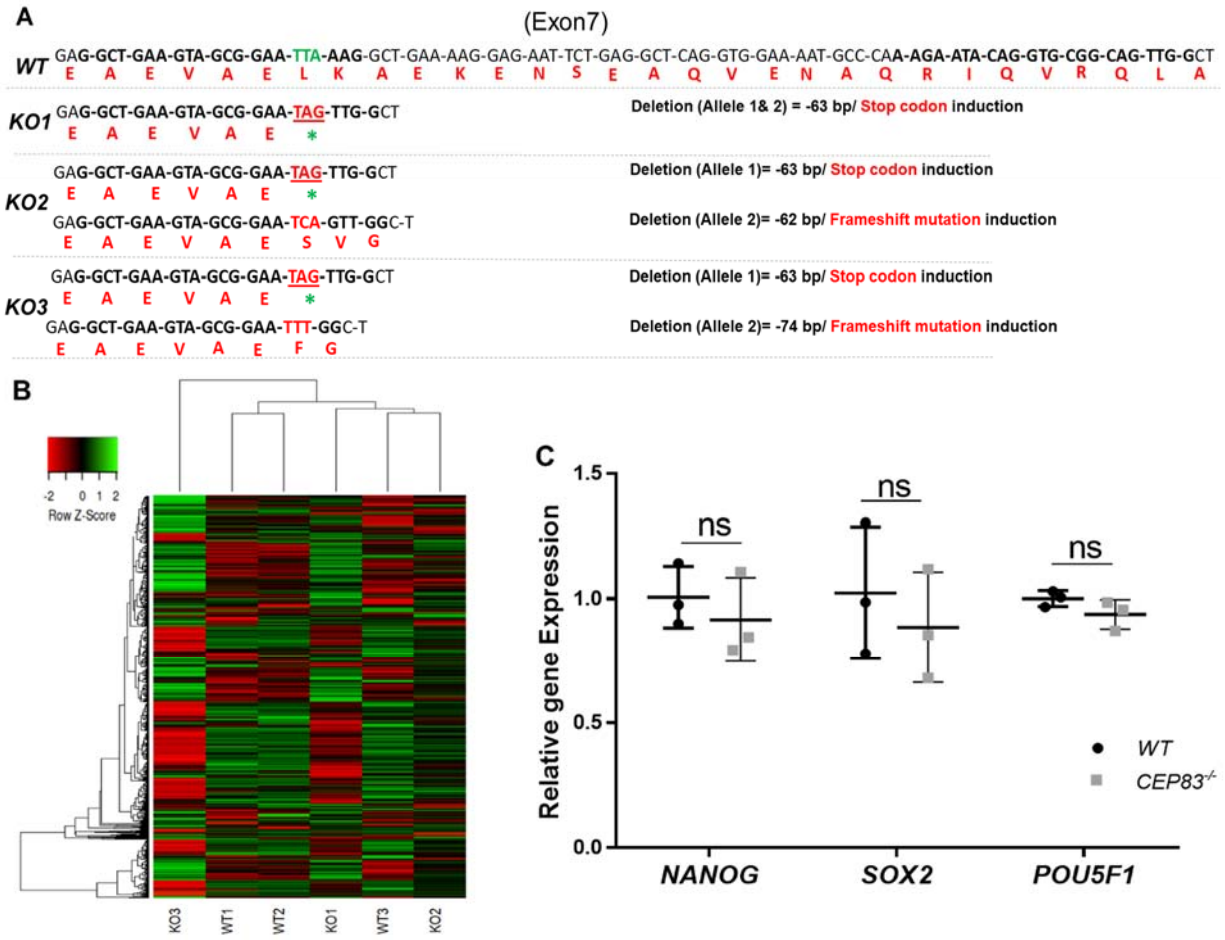

Figure 1- figure supplement 1: *CEP83*$^{-/-}$ hiPSCs retain global iPCS cell gene expression signatures and express pluripotency markers. (A) Alignment of the modified *KO* clones mRNA and expected amino acids sequences with *WT* revealed induction of stop codon on both strands of *KO1* clone. While *KO2* clone shows induction of stop codon on one allele and frameshift mutation within the second allele with 62 bp deletion. *KO3* clone sequence shows induction of stop codon on one allele and frameshift mutation with 74 bp deletion in the second allele. (B) Heatmap showing the expression of the top 1000 highly variable genes (see method, with a selection of TPM ≥ 10) within *WT* (*WT1, WT2*, and *WT3*) and CEP83$^{-/-}$ hiPSCs (*KO1, KO2*, and *KO3*) clones. Unbiased hierarchical clustering of clones indicates that gene expression similarity is not driven by WT or KO status. (C) RT-PCR shows no significant differences in the expression

of pluripotency markers *NANOG*, *SOX2*, and *POU5F1* between *WT* and *CEP83*$^{-/-}$ hiPSCs. TPM, Transcripts Per Million. n = 3 hiPSCs clones per group. Data are mean ± SD. ns, not significant.

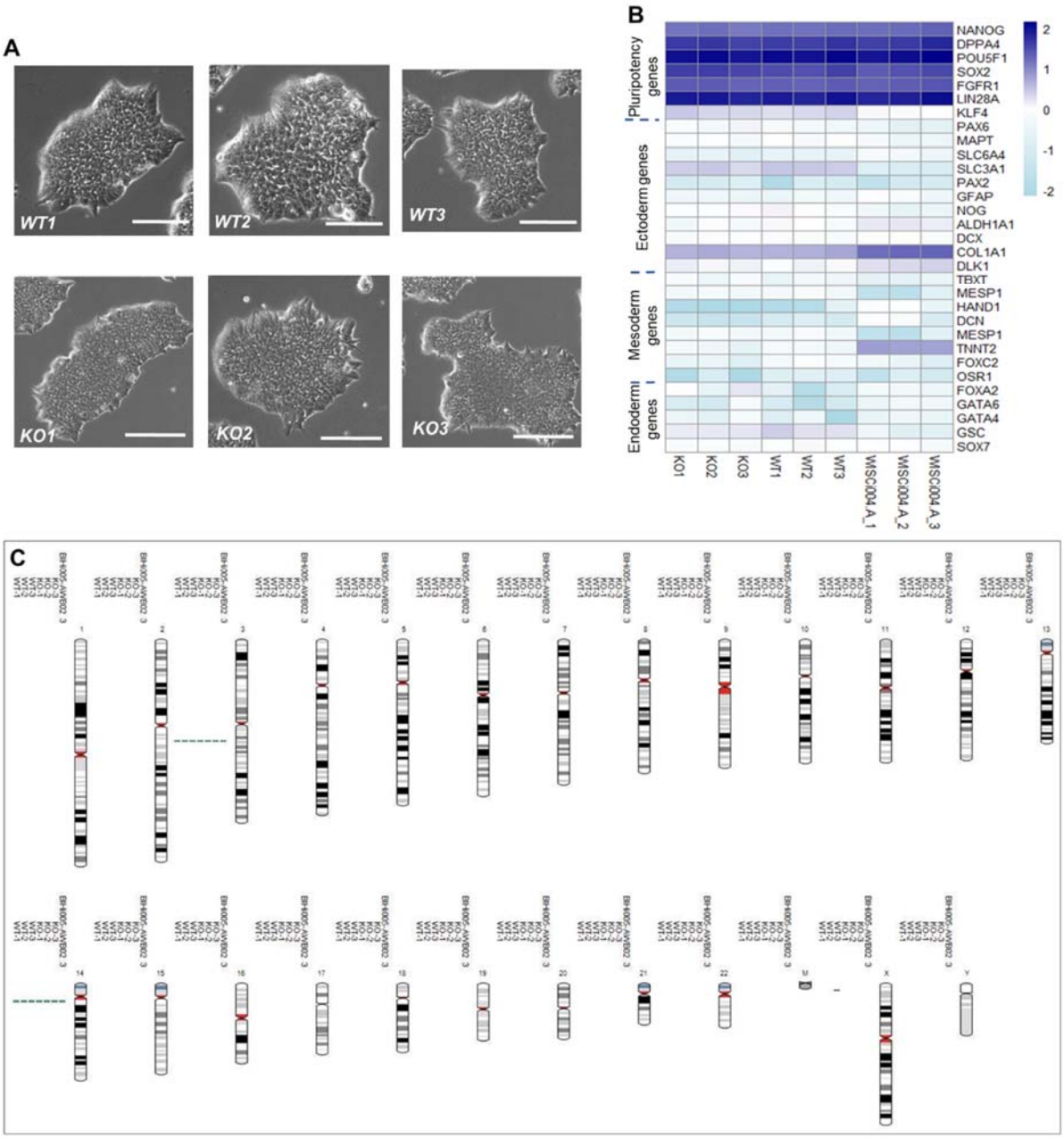

Figure 1- figure supplement 2: Phenotypical, molecular and genetic characterization of *CEP83*$^{-/-}$ hiPSCs versus the wildtype hiPSCs. (A) *CEP83*$^{-/-}$ hiPSCs clones (*KO1, KO2*, and *KO3*) show similar morphology to the *WT* clones (*WT1, WT2*, and *WT3*) under the bright field microscope, scale bar= 200 µm. (B) Using bulk RNA sequencing data, TPM values for marker

genes for pluripotency, ectodermal, mesodermal, and endodermal cells were plotted across the samples *(KO1, KO2, KO3, WT1, WT2*, and *WT3*). In addition, gene expression of the 6 samples was compared to three wildtype hiPSCs (WISCi004-A, also referred to as IMR90-4 iPS derived from female lung fbroblasts) that were previously published[1]. (C) The three *WT* clones, three *KO* clones, and the parental population were karyotyped using single nucleotide polymorphism (SNP) - analysis, demonstrating unaffected integrity of karyotypes. Two aberrations (one gain on Chr3 and one gain on Chr14) present in BIHi005-A were previously reported (https://hpscreg.eu/cell-line/BIHi005-A, Berlin Institute of Health Stem Cell Core Facility).

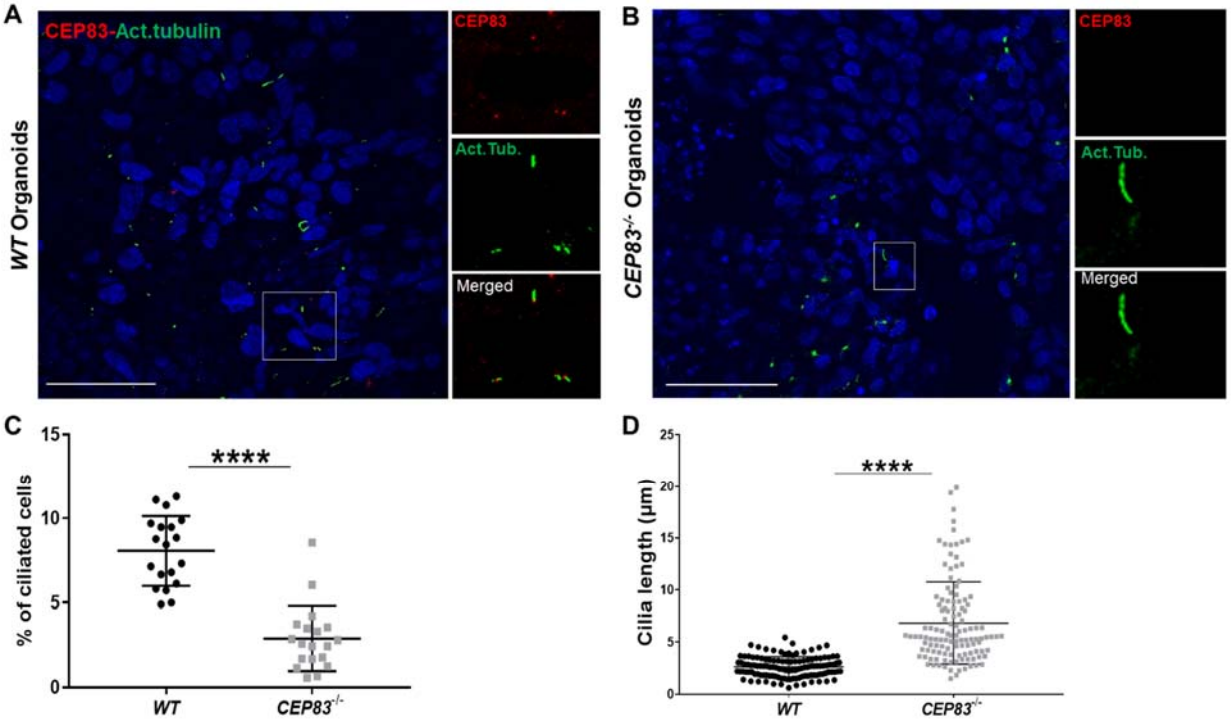

Figure 2- figure supplement 1: Loss of *CEP83* in organoids results in defective ciliogenesis. (A) Immunofluorescence staining of WT and CEP83$^{-/-}$ organoids for acetylated tubulin (green), CEP83 protein (red), and nuclear staining (DAPI). Note CEP83 localization at the base of the cilium in WT organoids. (B) Quantitative analysis of ciliated cells showing downregulation of the number of ciliated cells in CEP83$^{-/-}$ organoids, associated with longer cilium formation (C). n = 3 clones per group. Data are mean ± SD. ****P < 0.0001. Panel A: Bar = 50 µm.

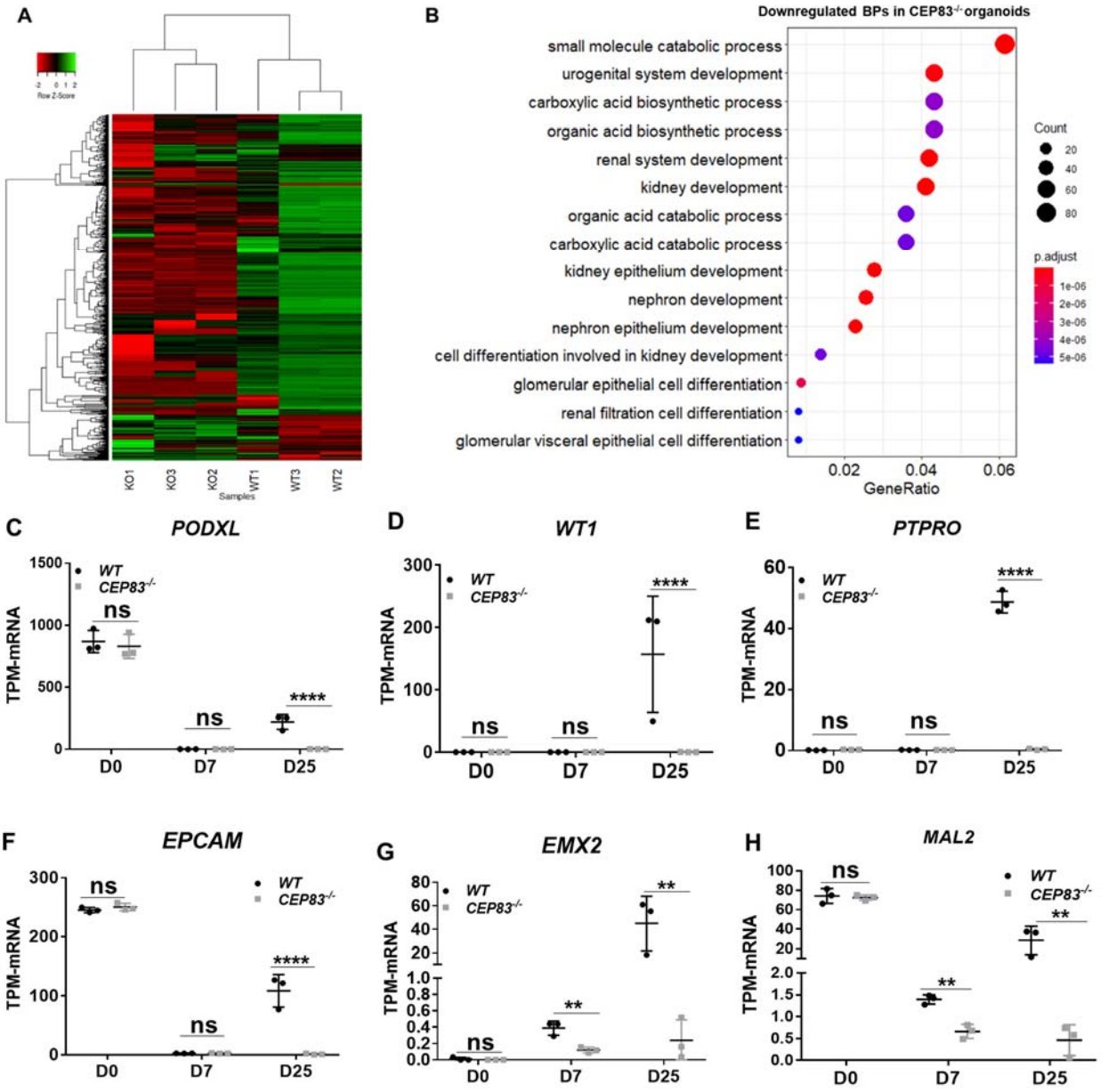

1009 **Figure 3- figure supplement 1: Bulk RNA-sequencing of organoids differentiated for 7+ (18)**
1010 **days indicates marked differences in global gene expression in *CEP83*$^{-/-}$ (*KO1-KO3*)**
1011 **compared to wildtype (*WT1-WT3*) organoids.** (A) Heatmap displaying the expression of the top
1012 1000 highly variable genes (see methods, TPM ≥ 10) within *WT* (*WT1, WT2, WT3*) and *CEP83*$^{-/-}$
1013 (*KO1, KO2, KO3*) organoids. Hierarchical clustering of clones indicating that global gene
1014 expression is profoundly different in *WT* and *KO* organoids. Ontology analysis of the biological
1015 processes (BPs) using the top 100 downregulated genes (based on fold change values) in *CEP83*$^{-}$

$^{-/-}$ organoids (TPM >2, fold change > 1.5, *P*-value calculated on log10 TPM < 0.05) using DOSE and cluster profile packages in R^2. The analysis shows downregulation of many biological processes associated with kidney development in *CEP83* mutated organoids, as shown in the dot plot (B). Bulk RNA sequencing shows downregulation of specific renal epithelial cells marker genes at day 25, including (C-E) *PODXL*, *WT1,* and *PTPRO* for podocytes. (F- H) *EPCAM*, *EMX2*, and *MAL2* marker genes for the distal nephron precursor cells. n = 3 clones per group. Data are mean ± SD. **P* < 0.05, ***P* < 0.01, and *****P* < 0.0001. ns= not significant.

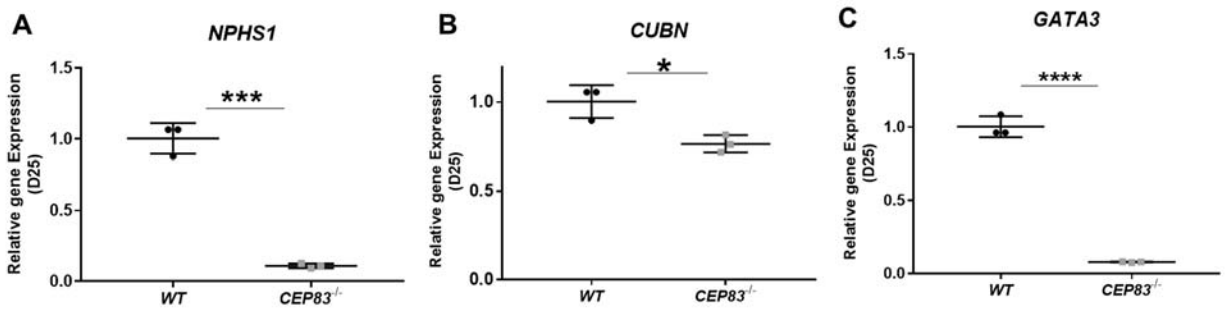

Figure 3- figure supplement 2: RT-PCR shows that the expression of some nephron epithelial markers, including *NPHS1* (Podocytes), *CUBN* (Proximal tubules), and *GATA3* (distal tubules and collecting duct) was significantly downregulated in *CEP83*$^{-/-}$ organoids. n = 3 clones per group. Data are mean ± SD. **P* < 0.05, ****P* < 0.001 and *****P* < 0.0001.

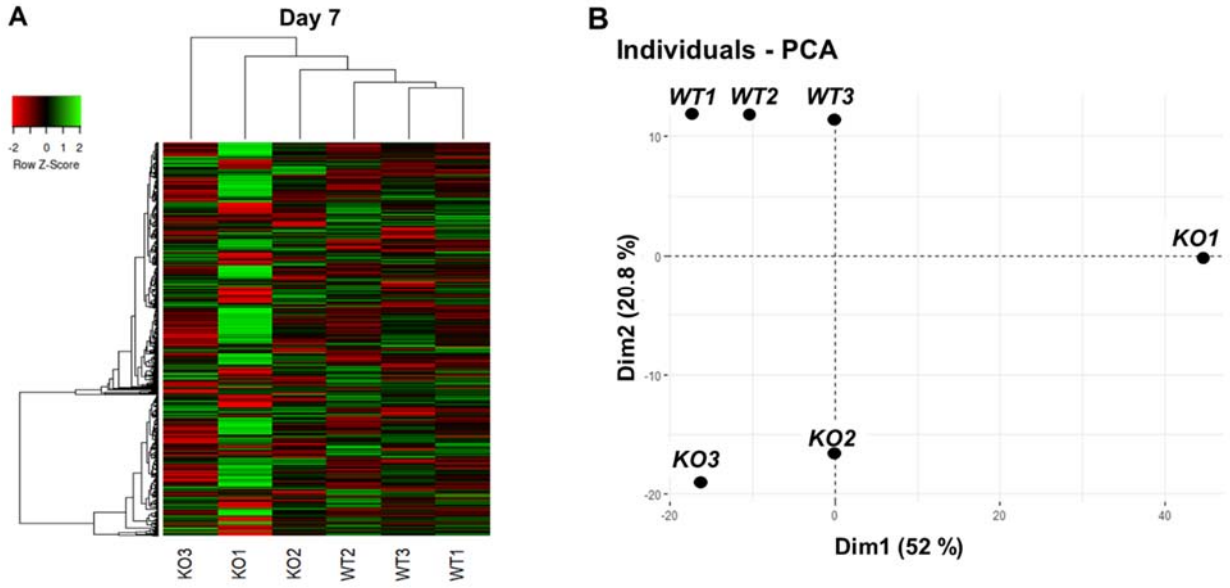

Figure 4- figure supplement 1: Bulk RNA sequencing shows mild overall gene expression differences between *WT* and *CEP83*-deficient cells at day 7 of differentiation. (A) Heat map of bulk RNA-seq data showing the most highly variable 1000 genes (see methods, maximum TPM ≥ 10) within wildtype (*WT1, WT2*, and *WT3*) and CEP83$^{-/-}$ (*KO1, KO2*, and *KO3*) clones at day 7 of differentiation. Unbiased hierarchical clustering of clones separates *CEP83*$^{-/-}$ and *WT* transcriptomes. (B) Principal component analysis (PCA) of *WT* (*WT1, WT2, WT3*) and *CEP83*$^{-/-}$ (*KO1, KO2, KO3*) cells at day 7 using the average gene expression of the top highly variable 1000 genes in bulk RNA sequencing data. The % variation explained by each PCA axis is indicated in brackets. PCA eigenvalues indicate that the principal components, Dim 1 (52%) and Dim 2 (20.8%), account for 85.3 % of the expression differences. Dim 1 separates the *KO1* sample from the other samples, while Dim 2 separates experiment 1 (*WT1, WT2, WT3*) and (*KO1, KO2, KO3*)

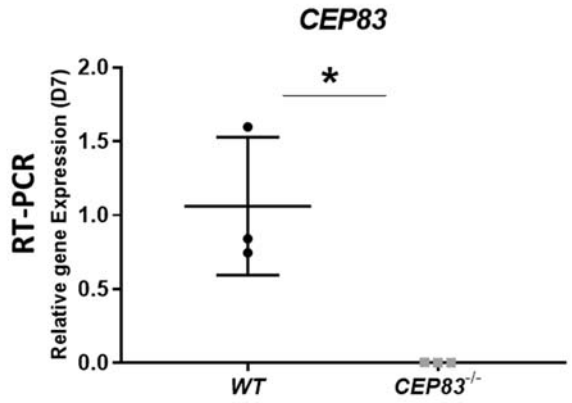

Figure 4- figure supplement 2: mRNA expression of *CEP83* was significantly downregulated in the *CEP83*$^{-/-}$ clones at day 7. The expression was investigated in bulk RNA seq data and confirmed by RT-PCR. n = 3 clones per group. Data are mean ± SD. **P* < 0.05

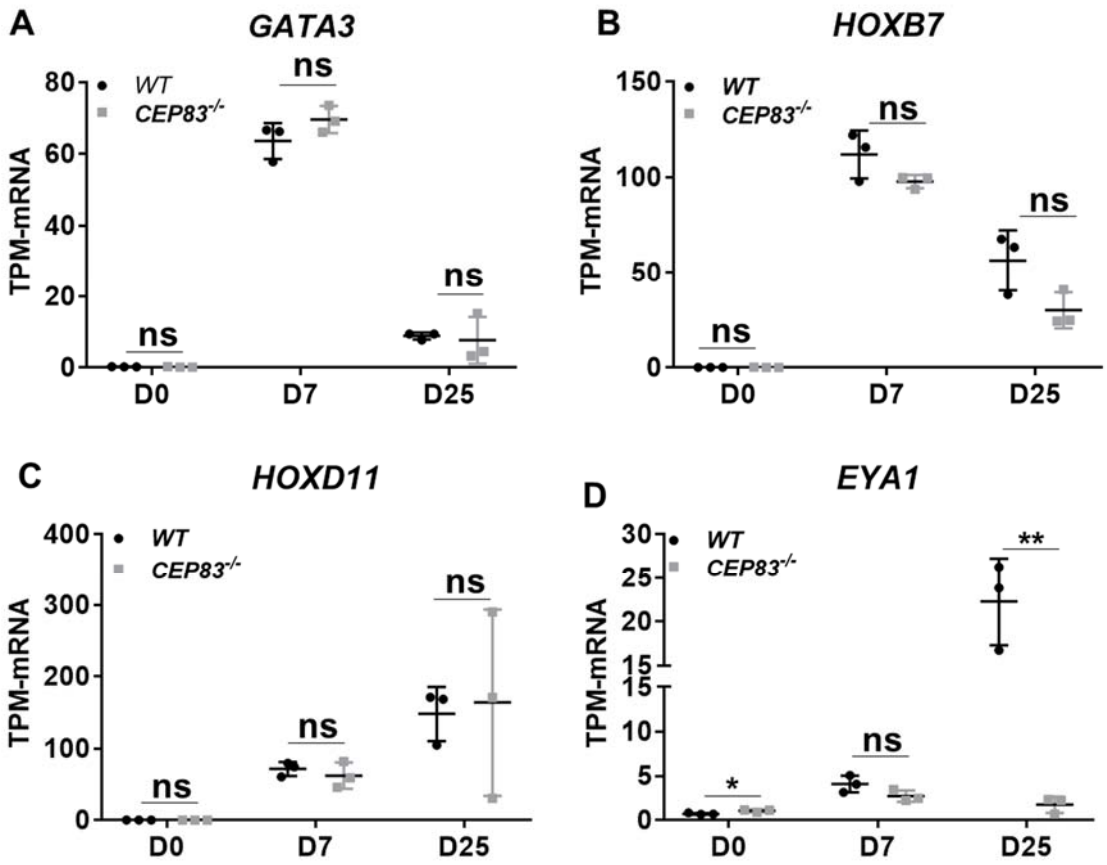

Figure 4- figure supplement 3: Expression of intermediate mesoderm marker genes in *WT* and *CEP83*$^{-/-}$ hiPSCs after 7 days of differentiation in a monolyer culture. (A-B) using Bulk

RNA sequencing data, the expression of Ureteric bud (UB) marker genes including *GATA3*, and *HOXB7* shows no significant change between WT and mutated cells at day 0, 7, and 25. While, (C-D) MM marker genes including *HOXD11* and *EYA1* show no significant difference between *WT* and *CEP83*$^{-/-}$ cells at day 0, 7, 25 except *EYA1* show significant downregulation in the mutated cells at day 25. n = 3 clones per group. Data are mean ± SD. ***P* < 0.01. ns= not significant.

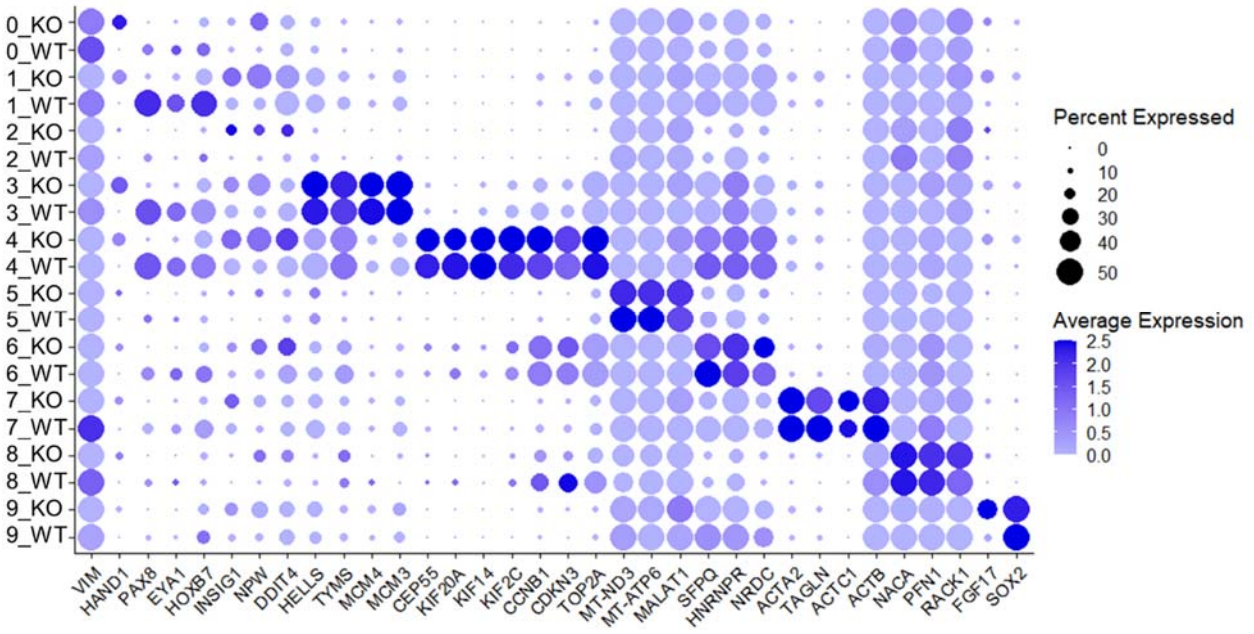

Figure 5- figure supplement 1: Dotplot shows the expression of marker genes of each cluster and the splitted expression per group (*WT* and *KO*). Cluster 0 (Mesenchymal cells) expresses mesenchymal genes, including *VIM* and *HAND1*. *VIM*, vimentin encodes an intermediate filament protein that plays a role in cytoskeleton organization[3,4]. The basic Helix-Loop-Helix (*bHLH*) transcription factor *HAND1* is expressed in the lateral plate mesoderm populations, in the developing heart, and in a subset of neural crest cells[5-7]. Thus, interestingly, the expression of *HAND1* is mainly represented by the *KO* cells in this cluster. Cluster 1 (Nascent nephron-1) shows upregulation of the nascent nephron marker genes, including *PAX8, EYA1*, and *HOXB7*. *PAX8* is a member of the *Pax2/5/8* family and is expressed during pro-, meso-, and metanephros development[8-10]. Interestingly, *PAX2-PAX8* double-mutant mice embryos exhibited impaired kidney development[11]. Deficiency of human *EYA1*, a homolog of the Drosophila

melanogaster gene eyes absent (eya), results in an inherited disorders branchio-oto-renal (BOR) syndrome in human with or without kidney defects[12,13]. *EYA1* knockout in mice results in complete renal agenesis[14]. *HOXB7* is one of HOX genes and is expressed in the mesonephros, ureter, and collecting system. Thus, *HOXB7* plays an essential role in kidney development. Overexpression of HOXB7 in mice causes renal duplications[15,16]. The expression of *PAX8*, *HOXB7*, and *EYA1* was observed additionally in clusters 3 and 4. Cluster 2 (Unknown cell type-1) is expressing *INSIG1*, *NPW*, and *DDIT4*. The insulin induced gene 1 (*INSIG1*) encodes a protein that mediates feedback control of cholesterol synthesis[17]. Neuropeptide W (*NPW*) is a gene that encodes peptides that bind and activate two G-protein coupled receptors: *GPR7* and *GPR8* in the central nervous system[18]. DNA damage inducible transcript 4 (*DDIT4*) gene is expressed under stress turning off the metabolic activity triggered by the mammalian target of rapamycin (mTOR)[19]. Most of the clusters express mainly cell cycle genes of different phases. Previous studies identified the cell cycle genes for each phase[20-23]. For instance, cluster 3 (S- Phase nascent nephron-2) mainly expresses the S- phase marker genes, including *HELLS, TYMS, MCM4*, and *MCM3* in addition to the nascent nephron marker genes. Cells of cluster 4 (M- Phase nascent nephron-3) express genes of the M- phase, including *CEP55, KIF20A, KIF14*, and *KIF2C*[24]. Besides, cluster 4 expresses the nascent nephron marker genes. In contrast, cluster 5 (damaged cells) includes the damaged cells that mainly express mitochondrial genes expression as *MT-ND3, MT-ATP6*, and *MALAT1*, and show the highest mitochondrial percent compared with other clusters. While, Clusters 6 and 8 express proliferative genes that reach their peak of expression in G2/M phase genes, including *CCNB1, CDKN3,* and *TOP2A*[20-23]. Besides the G2/M phase marker genes, cluster 6 (G2/M Phase unknown cell type-2) expresses *SFPQ, HNRNPR*, and *NRDC*. Splicing Factor Proline and Glutamine Rich (SFPQ) is a ubiquitous and abundant RNA-binding protein with multiple regulatory roles in the nucleus[25]. Heterogeneous Nuclear Ribonucleoprotein R (HNRNPR) promoted cancer cell proliferation by stabilizing the expression of *CCNB1* and *CENPF* mRNA levels and promoting transcription at the proto-oncogene c-fos[26,27]. Nardilysin Convertase

(*NRDC*) gene encodes an enzyme highly expressed in human developing adult brain[28]. We couldn't identify the type of cells of this cluster according to its gene expression profile. Cluster 7 (Actins enriched) expresses genes that encode actin proteins, including *ACTA2, TAGLN*, *ACTC1,* and *ACTB,* which are expressed in the cytoskeleton of the cell[29,30]. While, cluster 8 (G2/M Phase unknown cell type-3) upregulates *NACA, PFN1*, and *RACK1*. The nascent-polypeptide-associated complex alpha polypeptide (NACA) gene encodes a protein associated with basic transcription factor 3 (*BTF3*) and acts as a potent Suppressor of protein aggregation and aging-related proteinopathies[31]. Profilin 1 (PFN1) plays a crucial role in promoting actin polymerization in cells[32]. Invitro study showed that receptor inhibition for activated C kinase 1 (RACK1) could suppress cell proliferation and induce apoptosis[33]. While cluster 9 (*SOX2* enriched) is expressing *FGF17* and *SOX2*. Fibroblast growth factor 17 (*FGF17*), a gene expressed in the developing brain and involved in cerebellar vermis development[34]. Sex determining region Y-box 2 (*Sox2*) gene plays a critical role in maintaining stem cell pluripotency and differentiation of pluripotent stem cells into neural progenitor stem cells[35]. n = 2 clones per group.

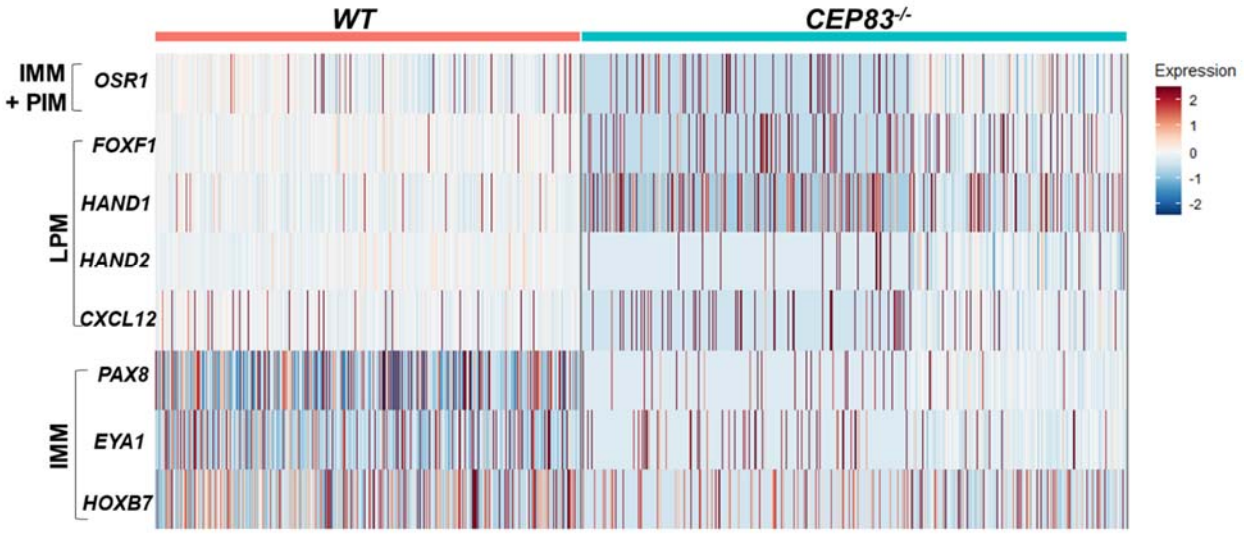

Figure 6- figure supplement 1: *CEP83*$^{-/-}$ cells upregulate LPM genes in mesenchymal cells cluster and nascent nephron progenitor clusters. The heatmap shows that the log fold change of the average expression (default setting in Seurat package) of LPM and IMM genes in the WT

cells (8,123 cell) and the knockout cells (10,431 cell) derived from the mesenchyme cells cluster (cluster 0) and the three nascent nephron clusters (1, 3, and 4). Scoring for cells expression for both LPM including: *FOXF1, HAND1, HAND2*, and *CXCL12,* and IMM genes including: *PAX8, EYA1*, and *HOXB7* were done in R. Each cell was scored 0- 4 for LPM genes expression. 0, 1, 2, 3 and 4 mean that cell express no LPM genes, 1 gene, 2 genes, 3 genes, and 4 genes, respectively. Statistical analysis comparing between LPM scores for *WT* and *KO* cells using wilcoxon rank sum test, showed that *KO* cells significantly upregulate the expression of LPM genes. The same scoring analysis was done for the expression of the IMM genes, where the cells got score from 0 to 3 for IMM genes expression. Interestingly, the *KO* cells showed significant downregulation of the IMM genes expression.

A

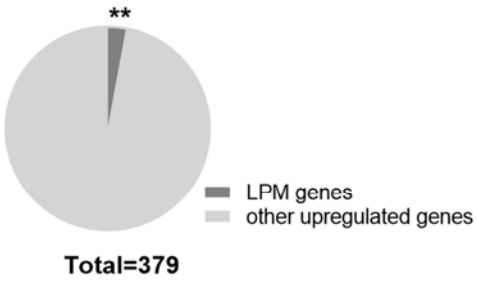

B

Overlapped genes between *CEP83*$^{-/-}$ organoids and developmental zebrafish LPM	
Zebrafish Gene	Human Gene
hand2	*HAND2*
cxcl12a	*CXCL12*
cxcl12b	*CXCL12*
sox7	*SOX7*
sox11a	*SOX11*
nap1l4a	*NAP1L3*
lmo2	*LMO2*
gata2a	*GATA2*
kctd12.2	*KCTD12*
pik3r3b	*PIK3R3*
znfl2a	*ZBTB2*

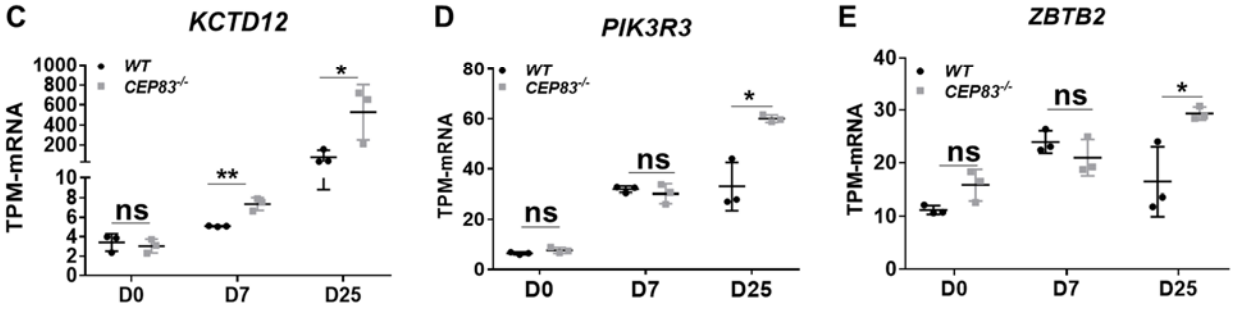

Figure 6- figure supplement 2: CEP83$^{-/-}$ organoids shows significant enrichment compared to developmental zebrafish LPM scRNA data. The expression of the upregulated genes by CEP83$^{-/-}$ organoids at day 25 were compared with the top 20 genes per cluster of zebrafish LPM scRNA data (Prummel et al., 2020). The analysis showed significant enrichment (A), with 11

zebrafish genes overlapped with 10 human genes (B). C, D, and E show the significant upregulation of three overlapped genes with zebrafish LPM including KCTD12, PIK3R3 and ZBTB2 respectively. n = 3 clones per group. Data are mean ± SD. *P < 0.05, and **P < 0.01. ns= not significant.

Supplemental Methods

hiPSCs Culture.

We used the human iPSC cell line BIHi005-A, which was generated from a healthy donor by the Berlin Institute of Health (BIH) and supplied by the stem cell core facility at Max Delbrück Center for Molecular Medicine (Berlin). The hiPSCs were maintained in 6-well plates (Corning®, 353046) coated with Matrigel (Corning®, 354277) and cultured in Essential 8 medium (E8, Gibco-Thermo Fisher Scientific, A1517001) supplemented with 10µM Y-27632 (Rocki, Wako, 253-00513). The cells were split twice per week using EDTA/PBS or Accumax™ (Stem cell technology, 07921).

CRISPR CAS9 Technology to generate CEP83$^{-/-}$ hiPSCs clones.

Clustered Regularly Interspaced Short Palindromic Repeats (CRISPR)-Cas9 technology was used to generate CEP83$^{-/-}$ hiPSCs clones. Two 20 bp-long CRISPR RNAs (crRNAs) were designed using CRISPOR software[36] to selectively target exon7: (5'-GGCTGAAGTAGCGGAATTAA-AGG-3'); (5'-AAGAATACAGGTGCGGCAGT-TGG-3'). The crRNAs were ordered from Integrated DNA Technologies (IDT). The crRNAs (IDT) were annealed in equimolar concentrations with trans-activating CRISPR RNA (tracrRNA) to form two guide RNAs (gRNA1 and gRNA2), which were then conjugated separately with Alt-R® S.p. Cas9 Nuclease V3 (1 µM concentration, IDT, 1081058) at

room temperature for 1 hour to form ribonucleoprotein (RNP) complexes (RNP1 and RNP2).

One day prior to transfection, hiPSCs were split using Accumax™ solution and cultured in an equal proportion of E8 medium and StemFlex™ medium (Thermo Fisher Scientific, A3349401). The hiPSCs were transfected using a Neon transfection system (Thermo Fisher Scientific, MPK5000). Immediately before the transfection, the cells were dissociated, collected, and resuspended in Resuspension Buffer (Buffer R), that included in Neon™ transfection 100 µl kit (Thermo Fisher Scientific, MPK10025)[37]. Cells were transfected in 3 ml Electrolytic buffer (Buffer E), that included in the neon transfection kit , and by using the Neon transfection system 10µl tip. The used Neon Transfection parameters were voltage (1200 V), width (30 ms), and pulse (1). The transfected cells were cultured in StemFlex™ Medium with Rocki for 48 hours.

Then, quick DNA extraction and PCR were then done to test transfection efficiency according to the manufacturer's instructions using Phire™ Tissue Direct PCR Master Mix (Thermo Scientific, F170S). The size of the PCR products were visualized on 1.5% agarose gel. After confirming the transfection's success in the knockout cells, as shown in **Figure 1B**, the cells were dissociated and seeded at low densities for 24 hours. Then, twenty-four single cells were picked under a picking hood S1 (stem cell core facility-MDC, Buch) and cultured in StemFlex™ medium for two weeks. The clones were then tested for CEP83 mutation on the DNA level by PCR using Phire™ Tissue Direct PCR Master Mix. Finally, the selected clones were expanded and frozen in the Bambanker medium (Nippon Genetics, BB01) for further characterization. The selected clones were characterized for the mutation induction on the DNA, protein, and RNA level.

Differentiation Protocol.

We used the protocol of ***Takasato*** to differentiate the hiPSCs into nephron organoids[38], the experiment was performed using three replicates per each group wildtype hiPSCs (*WT1*, *WT2*, and *WT3*) and *CEP83*$^{-/-}$ hiPSCs (*KO1*, *KO2*, and *KO3*). Two days prior to the differentiation, cultured hiPSCs on matrigel with 70-80% density were prepared for the differentiation. The cells wrere washed twice with 1x Dulbecco's PBS (Thermo Fisher Scientific,14190-250), then cells were trypsinized using 1x Trypl E Select (Thermo Fisher Scientific, 12563011). Cells were incubated at 37 °C for 3 minutes. Then, DMEM/F-12 medium (Thermo Fisher Scientific, 11320-033) were added on the cells to neutralize Trypl E. The cell suspension was were mixed by pipetting (pipetting is maximum twice), then centrifuged at 300g for 5 minutes. The cell pellet was washed and resuspended in 1 ml of E8 medium. Then the cells was counted using Countess® chamber slide and Countess II Automated Cell Counter (Thermo Fisher Scientific). Then cells were centrifuged and resuspended in E8 media supplemented with 10μM Rocki. Lastly, cells were cultured on a prepared coated matrigel six well culture plates to obtain a density of 15 × 10^3 cells per $cm^{2.}$, and incubated overnight at 37°C CO_2 incubator for 48 h with daily medium change.

Immediately before the differentiation, the cells were checked under microscope. Cells with 40–50% confluency were used for the differentiation. The E8 medium was changed into APEL2 medium (Stem Cell Technologies, 05270) with 5% Protein Free Hybridoma Medium II (PFHMII, GIBCO, 12040077) and 8 μM CHIR99021 (2 ml medium per a well

of 6- well plate). Cells were incubated in a 37 °C CO_2 incubator for **5d**, with medium refreshing every 2d. Following the CHIR99021 phase, the medium was changed into double volume of APEL2 medium (4 ml medium per a well of 6- well plate) supplemented with 200 ng/ml FGF9 (R&D, 273-F9-025) and 1 μg/ml heparin (Sigma Aldrich, H4784-250MG), and were incubated in a 37°C CO_2 incubator.

On day 7 of differentiation, the cells were washed, trypsinizied with trypsin EDTA (0.05%), and incubated at 37°C for 3 min. Then, the cell suspension was transferred to a 50-ml tube containing 9 ml of MEF conditioned medium (R&D, AR005) to neutralize the trypsin. The cells were centrifuged and resuspend in APEL2 medium. Using a hemocytometer, the cells were counted and the cell suspension was divided to achieve 1×10^6 cells (organoid) per 1.5 ml tube. All the tubes were centrifuged at 400xg for 3 min at RT. During centrifugation, Six-well Transwell cell culture plates (Corning-Sigma Aldrich, CLS3450-24EA) were prepared by adding 1.2 ml of APEL2 supplmented with 5 μM CHIR99021 to each well. Cell pellets were picked up by using a P1,000 or P200 wide-bore tip. Pellets were carefully seeded onto the six-well Transwell membrane with minimal APEL2 medium carryover, and incubated at 37°C for 1h. Then the medium were changed into APEL2 medium supplemented with 200 ng/ml FGF9 plus 1 μg/ml heparin for further 5 days, with medium refreshing every 2 days. Finally, the medium to APEL2 medium with only heparin for further 13 days, with medium refreshing every 2 days.

DNA isolation and Polymerase Chain Reaction (PCR).

Cultured *WT* and *CEP83*$^{-/-}$ hiPSCs were washed, scrapped gently using a cell scraper (VWR, part of Avantor, 734-2602), collected with a maximum $5x10^6$ cell/ml for proper DNA extraction. The DNA was extracted using DNeasy Blood & Tissue Kits (Qiagen, 69504)

following the manufacturer's instructions. The concentrations and quality of the DNA were evaluated using Nanodrop (Thermo Scientific, Waltham, MA; USA). To detect CEP83 expression, 200 µg DNA was amplified by a standard Polymerase Chain Reaction (PCR) using Phusion high-fidelity DNA polymerase (Biolabs, New England, M0530). The master mix was calculated according to the manufacturer's instructions. Primers are designed using Primer3 webtool, Table S1. PCR was carried out in a thermocycler as follow: initial denaturation at 98°C for 30 sec, 35 to 40 cycles of 30 sec at 98°C, 30 sec at 63.5 °C and 30 sec at 72°C; final elongation step at 72°C for 10 min. The PCR results were checked on 1.5% agarose gel and analyzed using a BioDoc Analyze dark hood and software system (Biometra).

RNA isolation, RNA Sequencing, and Quantitative PCR (qPCR).

Total RNA was isolated from the cells at three time points: day 0 (hiPSCs), day 7 (IMM), and day 25 (organoids) with a maximum of $1x10^7$ cells using RNAasy Mini Kit (QIAGEN, Hilden, Germany, 74104,) following the manufacture instructions. The RNA was treated with RNase-free DNase I (QIAGEN, 79254) for 15 minutes at room temperature during the extraction. The concentration, quality, and integrity of the extracted RNA were evaluated using Nanodrop (Thermo Scientific, Waltham, MA; USA), an Agilent 2100 Bioanalyzer, and the Agilent RNA 6000 Nano kit (5067-1511, Agilent Technologies). More than 0.4 µg total RNA with high integrity (more than 6.8) and high purity (OD260/280 = 1.8-2.2 and OD260/230 ≥ 1.8) were collected and sent for Illumina NovaSeq 6000RNA sequencing by Novogene. RNA-Seq library preparation and next-generation sequencing: cDNA libraries with paired-end 150 bp enriched were prepared by Novogene. Firstly the mRNA was randomly fragmentated and supplemented with oligo (dT) beads. Then cDNA

synthesis were done using the random hexamers and reverse transcriptase. Secondly, second-strand synthesis was done using: a custom second-strand synthesis buffer from Illumina, deoxyribose nucleoside triphosphates (dNTPs), RNase H and E.coli polymerase I. The final obtained cDNA library was purified, terminally repaired, A-tailed, ligated to sequencing adapters, size-selected, and PCR-enriched. Quantification of library concentration was performed using a Qubit 2.0 fluorometer. Library size was measured by Agilent 2100 bioanalyzer and was quantified by qPCR (library activity > 2 nM). Libraries were sequenced on Illumina NovaSeq 6000 S4 flow cells (paired end, 150bp).

Raw data were transformed to sequenced reads, and recorded in a FASTQ file. FASTQ files were aligned to build 19 of the human genome provided by the Genome Reference Consortium (GRCh19) performed by Christian Hinze using TOPHAT2 aligner tool[39]. Up to 4 mismatches with the reference genome were accepted. Raw counts were obtained using featureCounts[40]. Mutation visualization in the knockout samples was performed using the Integrative Genomic Viewer (IGV) tool[41]. For gene expression analysis reads were normalized to the sequence length and transcripts per million (TPM) values were calculated[42]. TPM values of the samples were used to plot heatmaps and for PCA analysis based on Pearson correlation, using R (R Development Core Team, 4.0.4)

500 ng of RNA was reverse transcribed using the RevertAid First Strand cDNA synthesis kit (Thermo Scientific, K1622) according to the manufacturer's instructions. The qPCR was carried out using the Fast Universal SYBR Green Master Mix (ROX, Roche Diagnostics, 04 913 850 001,) according to the manufacturer's instructions. For expression analysis, relative mRNA expression levels were normalized for GAPDH mRNA expression and calculated according to the ΔΔCt method. All primer pairs were

designed using the free-online primer design tool Primer3, purchased at BioTeZ (Berlin, Germany), and sequences are shown in (Table S1). Statistical significance of differences between two groups (WT and KO) was analyzed using two-sided Student's t-test.

Single cell RNA (scRNA) experiment.

Cells isolation and preparation

The differentiated hiPSCs to intermediate mesodermal cells were collected at day 7 of the differentiation from two different experiments. The cells of the first experiment were derived from *WT1* and *KO1* differentiated hiPSCs, while the second experiment comprises the differentiated cells of *WT2* and *KO2* cells. The cells were washed twice with 1X DPBS and dissociated with Accumax for 7 min at 37 °C. Cells were centrifuged at 350 × g for 5 min, and resuspended in 1X DPBS. Then, cells were filtered a 40 µm filter (Corning, 352340), counted (10,000 cells per sample), and checked for viability using Trypan blue staining.

Protein extraction and Immunoblotting.

Protein extraction: Up to $1*10^6$ hiPSCs per sample (*WT1*, *WT2*, *WT3*, *KO1*, *KO2*, and *KO3*) were washed with cold 1xPBS, then centrifuged at 3500 g for 5 minutes. Next, the cell pellet was resuspended in pre-ice cold 100 µl of radioimmunoprecipitation assay (RIPA) buffer (Sigma-Aldrich, R0278) supplemented with protease inhibitor (Roche, 11697498001) and maintained with constant agitation for 30 min at 4°C. Then the suspension was centrifuged at 4°C for 20 minutes at 12,000 rpm. The supernatant was collected as protein extract and quantified using BCA Protein Assay (Thermo Scientific, 23228).

Immunoblotting: 30 µg of the extracted protein in RIPA buffer were mixed with 1x reducing (10% b-mercaptoethanol) NuPAGE loading buffer (Life Technologies, Carlsbad, CA). After denaturation at 70°C for 10 min. The protein was loaded on a precast polyacrylamide NuPage 4-12% Bis-Tris protein gel (Invitrogen, Carlsbad, CA, USA) and 1x MOPS (1M MOPS, 1M TrisBase, 69.3mM SDS, 20.5mM EDTA) to be separated according to the length using SDS -PAGE (100V, 200mA, 2h). Proteins were blotted on 0.45 µm pore size Immobilon-P Polyvinylidene difluoride (PVDF) membrane (EMD Millipore, Billerica, MA; USA). The membrane was pre-activated for 20 sec in methanol and equilibrated in 1X NuPage Transfer buffer (1.25 mM bicine, 1.25 mM BisTris, 0.05 mM EDTA, and 10% ethanol) for 30 min at RT. The membrane was blocked in 5% bovine serum albumin for 1 h at RT and incubated overnight at 4°C with primary antibodies: Anti-CEP83 produced in rabbit (1:500, Sigma-Aldrich) and Anti-α-Tubulin produced in mouse (1:500, T9026, Sigma-Aldrich). The membrane was incubated for 1 h at RT with horseradish peroxidase-conjugated secondary antibodies (Sigma-Aldrich, Saint Louis, MO, USA) with 1:2000 dilution. Chemiluminescent reagent (Super Signal–West Pico; Thermo Scientific, Waltham, MA; USA) was used to detect the proteins. The spectra^{TM} Multicolor Broad Range Protein Ladder (Thermo Fisher Scientific, USA) was used to evaluate the molecular weight of corresponding protein bands.

Histology and Immunofluorescence (IF) staining.

After organoid fixation in BD Cytofix buffer (554655, BD Biosciences) for 1 hour on ice, the organoids were gradually dehydrated in increasing ethanol concentrations for 15 minutes each. Then organoids were cleared in xylene for three times 20 minutes each. After infiltration with melted paraffin at 65°C three times for 30 minutes each, the

organoids were embedded in paraffin and processed in 3.5 µm-thick sections using a HM 355S microtome. The sections were deparaffinized, dehydrated, and stained with hematoxylin (Sigma-Aldrich, Saint Louis, MO) for 3 minutes and in 1% eosin (Sigma-Aldrich) for 2 minutes. The sections were mounted using Kaiser's glycerol gelatin-based mounting medium. Images were captured with a Leica CTR 6000 microscope (Leica Biosystems, Wetzlar, Germany).

For immunostsining, cultured cells (D7) and organoids (D25) were fixed with BD Cytofix for 10 miuntes on ice. Then cells were permeabilized with BD Perm/Wash (554723, BD Biosciences), twice, 15 minutes per each. Cells were blocked with blocking solution (1% BSA + 0.3% triton-X-100 in 1X DPBS) for 2 hours at RT or overnight at 4°C. Cells were incubated overnight at 4°C with primary antibodies (table S2). Cells were then washed twice (10 min each) and incubated with fluorescence-labeled secondary antibodies with 1:500 dilution including Cy3, Cy5, Alexa488, and Alexa647 (Jackson ImmunoResearch, Newmarket, UK) and Cy3 Streptavidin (Vector lab, Burlingame, USA) overnight at 4°C. DAPI was then used for nuclear staining (Cell signaling Technology, Danvers, MA, USA) with 1:300000 dilution for 1 hour at RT. Finally, cells were mounted with Dako fluorescent mounting medium (Agilent Technologies). The images were taken using a SP8 confocal microscope (Carl Zeiss GmbH, Oberkochen, Germany). All the quantitative analyses of the taken images were performed using ImageJ (1.48v; National Institutes of Health, Bethesda, MD) software.

Supplemental Tables:

1324 **Table S1: Primers list used in the qPCR.**

Gene	Forward primer sequence (5' →3')	Reverse primer sequence (5' →3')
CEP83	AGACAGCAAACGAGTGGAAC	GGATCTGACTGTAGCCTGCA
OSR1	CCTTCCTTCAGGCAGTGAAC	CGGCACTTTGGAGAAAGAAG
GAPDH	AGCCACATCGCTCAGACAC	GCCCAATACGACCAAATCC
OCT4/POU5F1	AGCAAAACCCGGAGGAGT	CCACATCGGCCTGTGTATATC
NANOG	AAGGCCTCAGCACCTACCTA	ATTGGAAGGTTCCCAGTCGG
SOX2	CAAAAATGGCCATGCAGGTT	AGTTGGGATCGAACAAAAGCTATT
HOXD11	CAGCAGCGCAGTTGCC	CGGTCAGTGAGGTTGAGCAT
EYA1	AACAGCTCACCGTATCCAGC	TGTGCTGTACTCTGCTGTGG
GATA3	GCCCCTCATTAAGCCCAAG	TTGTGGTGGTCTGACAGTTCG
HOXB7	AAGCTCAGGAACTGACCGC	CCCTGTCTTGGCCGGTG
PODXL	CAACCCGGCCCAAGATAAGT	GGCAGGGAGCTTAGTGTGAA
CUBN	CTGCCGTCTTCCAGTCTCAG	ACAGCGGAACGAGCTTCTAA

1325

1326 **Table S2: Primary antibodies used in IF staining.**

Antibody	Dilution	Company
Monoclonal Anti-Tubulin, acetylated antibody (T6793). mouse	IF: 1:2000	Sigma-Aldrich, Saint Louis, MO, USA
anti-Cdh1	IF: 1:200	BD Bioscience, San Jose, CA, USA
Lotus tetragonolobus lectin (LTL)	IF: 1:200	Vector lab, Burlingame, USA
Anti-NPHS1	IF: 1:300	R&D System, Minneapolis, MN, USA
Anti- CEP83	IF: 1:200	Sigma-Aldrich, Saint Louis, MO, USA

1327

Supplemental References:

1 Hariharan, K., Stachelscheid, H., Rossbach, B., Oh, S.-J., Mah, N., Schmidt-Ott, K., Kurtz, A. & Reinke, P. Parallel generation of easily selectable multiple nephronal cell types from human pluripotent stem cells. *Cellular and Molecular Life Sciences* **76**, 179-192, doi:10.1007/s00018-018-2929-2 (2019).

2 Yu, G., Wang, L. G., Han, Y. & He, Q. Y. clusterProfiler: an R package for comparing biological themes among gene clusters. *Omics : a journal of integrative biology* **16**, 284-287, doi:10.1089/omi.2011.0118 (2012).

3 May, C. D., Sphyris, N., Evans, K. W., Werden, S. J., Guo, W. & Mani, S. A. Epithelial-mesenchymal transition and cancer stem cells: a dangerously dynamic duo in breast cancer progression. *Breast Cancer Research* **13**, 1-10 (2011).

4 Bollong, M. J., Pietilä, M., Pearson, A. D., Sarkar, T. R., Ahmad, I., Soundararajan, R., Lyssiotis, C. A., Mani, S. A., Schultz, P. G. & Lairson, L. L. A vimentin binding small molecule leads to mitotic disruption in mesenchymal cancers. *Proceedings of the National Academy of Sciences* **114**, E9903-E9912, doi:10.1073/pnas.1716009114 (2017).

5 Firulli, A. B., McFadden, D. G., Lin, Q., Srivastava, D. & Olson, E. N. Heart and extra-embryonic mesodermal defects in mouse embryos lacking the bHLH transcription factor Hand1. *Nature genetics* **18**, 266-270 (1998).

6 Morikawa, Y. & Cserjesi, P. Extra-embryonic vasculature development is regulated by the transcription factor HAND1. *Development (Cambridge, England)* **131**, 2195-2204, doi:10.1242/dev.01091 (2004).

7 Barbosa, A. C., Funato, N., Chapman, S., McKee, M. D., Richardson, J. A., Olson, E. N. & Yanagisawa, H. Hand transcription factors cooperatively regulate

development of the distal midline mesenchyme. *Dev Biol* **310**, 154-168, doi:10.1016/j.ydbio.2007.07.036 (2007).

8 Plachov, D., Chowdhury, K., Walther, C., Simon, D., Guenet, J.-L. & Gruss, P. Pax8, a murine paired box gene expressed in the developing excretory system and thyroid gland. *Development (Cambridge, England)* **110**, 643-651 (1990).

9 Pfeffer, P. L., Gerster, T., Lun, K., Brand, M. & Busslinger, M. Characterization of three novel members of the zebrafish Pax2/5/8 family: dependency of Pax5 and Pax8 expression on the Pax2. 1 (noi) function. *Development (Cambridge, England)* **125**, 3063-3074 (1998).

10 Mansouri, A., Chowdhury, K. & Gruss, P. Follicular cells of the thyroid gland require Pax8 gene function. *Nature genetics* **19**, 87-90 (1998).

11 Bouchard, M., Souabni, A., Mandler, M., Neubüser, A. & Busslinger, M. Nephric lineage specification by Pax2 and Pax8. *Genes & development* **16**, 2958-2970 (2002).

12 Vincent, C., Kalatzis, V., Abdelhak, S., Chaïb, H., Compain, S., Helias, J., Vaneecloo, F.-M. & Petit, C. BOR and BO syndromes are allelic defects of EYA1. *European Journal of Human Genetics* **5**, 242-246 (1997).

13 Kumar, S., Kimberling, W. J., Weston, M. D., Schaefer, B. G., Berg, M. A., Marres, H. A. & Cremers, C. W. Identification of three novel mutations in human EYA1 protein associated with branchio-oto-renal syndrome. *Human mutation* **11**, 443-449 (1998).

14 Xu, P.-X., Adams, J., Peters, H., Brown, M. C., Heaney, S. & Maas, R. Eya1-deficient mice lack ears and kidneys and show abnormal apoptosis of organ primordia. *Nature Genetics* **23**, 113-117, doi:10.1038/12722 (1999).

15 Patterson, L. T. & Potter, S. S. Atlas of Hox gene expression in the developing kidney. *Developmental Dynamics* **229**, 771-779, doi:https://doi.org/10.1002/dvdy.10474 (2004).

16 Rojek, A., Füchtbauer, E.-M., Kwon, T.-H., Frøkiær, J. & Nielsen, S. Severe urinary concentrating defect in renal collecting duct-selective AQP2 conditional-knockout mice. *Proceedings of the National Academy of Sciences* **103**, 6037-6042, doi:10.1073/pnas.0511324103 (2006).

17 Liu, X., Li, Y., Wang, L., Zhao, Q., Lu, X., Huang, J., Fan, Z. & Gu, D. The INSIG1 gene, not the INSIG2 gene, associated with coronary heart disease: tagSNPs and haplotype-based association study. The Beijing Atherosclerosis Study. *Thromb Haemost* **100**, 886-892 (2008).

18 Shimomura, Y., Harada, M., Goto, M., Sugo, T., Matsumoto, Y., Abe, M., Watanabe, T., Asami, T., Kitada, C., Mori, M., Onda, H. & Fujino, M. Identification of neuropeptide W as the endogenous ligand for orphan G-protein-coupled receptors GPR7 and GPR8. *J Biol Chem* **277**, 35826-35832, doi:10.1074/jbc.M205337200 (2002).

19 Tirado-Hurtado, I., Fajardo, W. & Pinto, J. A. DNA Damage Inducible Transcript 4 Gene: The Switch of the Metabolism as Potential Target in Cancer. *Frontiers in Oncology* **8**, doi:10.3389/fonc.2018.00106 (2018).

20 Kowalczyk, M. S., Tirosh, I., Heckl, D., Rao, T. N., Dixit, A., Haas, B. J., Schneider, R. K., Wagers, A. J., Ebert, B. L. & Regev, A. Single-cell RNA-seq reveals changes in cell cycle and differentiation programs upon aging of hematopoietic stem cells. *Genome research* **25**, 1860-1872 (2015).

21 Subramanian, A., Sidhom, E.-H., Emani, M., Vernon, K., Sahakian, N., Zhou, Y., Kost-Alimova, M., Slyper, M., Waldman, J., Dionne, D., Nguyen, L. T., Weins, A., Marshall, J. L., Rosenblatt-Rosen, O., Regev, A. & Greka, A. Single cell census of human kidney organoids shows reproducibility and diminished off-target cells after transplantation. *Nature Communications* **10**, 5462, doi:10.1038/s41467-019-13382-0 (2019).

22 Low, J. H., Li, P., Chew, E. G. Y., Zhou, B., Suzuki, K., Zhang, T., Lian, M. M., Liu, M., Aizawa, E. & Esteban, C. R. Generation of human PSC-derived kidney organoids with patterned nephron segments and a de novo vascular network. *Cell Stem Cell* **25**, 373-387. e379 (2019).

23 Knapp, K. M., Jenkins, D. E., Sullivan, R., Harms, F. L., von Elsner, L., Ockeloen, C. W., de Munnik, S., Bongers, E. M. H. F., Murray, J., Pachter, N., Denecke, J., Kutsche, K. & Bicknell, L. S. MCM complex members MCM3 and MCM7 are associated with a phenotypic spectrum from Meier-Gorlin syndrome to lipodystrophy and adrenal insufficiency. *European Journal of Human Genetics*, doi:10.1038/s41431-021-00839-4 (2021).

24 Miki, H., Setou, M., Kaneshiro, K. & Hirokawa, N. All kinesin superfamily protein, KIF, genes in mouse and human. *Proceedings of the National Academy of Sciences* **98**, 7004-7011, doi:10.1073/pnas.111145398 (2001).

1418 25 Lim, Y. W., James, D., Huang, J. & Lee, M. The Emerging Role of the RNA-Binding
1419 Protein SFPQ in Neuronal Function and Neurodegeneration. *International journal*
1420 *of molecular sciences* **21**, doi:10.3390/ijms21197151 (2020).
1421 26 Chen, E. B., Qin, X., Peng, K., Li, Q., Tang, C., Wei, Y. C., Yu, S., Gan, L. & Liu,
1422 T. S. HnRNPR-CCNB1/CENPF axis contributes to gastric cancer proliferation and
1423 metastasis. *Aging (Albany NY)* **11**, 7473-7491, doi:10.18632/aging.102254 (2019).
1424 27 Fukuda, A., Nakadai, T., Shimada, M. & Hisatake, K. Heterogeneous nuclear
1425 ribonucleoprotein R enhances transcription from the naturally configured c-fos
1426 promoter in vitro. *J Biol Chem* **284**, 23472-23480, doi:10.1074/jbc.M109.013656
1427 (2009).
1428 28 Bernstein, H. G., Stricker, R., Dobrowolny, H., Trübner, K., Bogerts, B. & Reiser,
1429 G. Histochemical evidence for wide expression of the metalloendopeptidase
1430 nardilysin in human brain neurons. *Neuroscience* **146**, 1513-1523,
1431 doi:10.1016/j.neuroscience.2007.02.057 (2007).
1432 29 Bertola, L. D., Ott, E. B., Griepsma, S., Vonk, F. J. & Bagowski, C. P.
1433 Developmental expression of the alpha-skeletal actin gene. *BMC evolutionary*
1434 *biology* **8**, 166-166, doi:10.1186/1471-2148-8-166 (2008).
1435 30 Kim, H.-R., Kwon, M.-S., Lee, S., Mun, Y., Lee, K.-S., Kim, C.-H., Na, B.-R., Kim,
1436 B. N. R., Piragyte, I., Lee, H.-S., Jun, Y., Jin, M. S., Hyun, Y.-M., Jung, H. S., Mun,
1437 J. Y. & Jun, C.-D. TAGLN2 polymerizes G-actin in a low ionic state but blocks
1438 Arp2/3-nucleated actin branching in physiological conditions. *Scientific Reports* **8**,
1439 5503, doi:10.1038/s41598-018-23816-2 (2018).

31 Shen, K., Gamerdinger, M., Chan, R., Gense, K., Martin, E. M., Sachs, N., Knight, P. D., Schlömer, R., Calabrese, A. N., Stewart, K. L., Leiendecker, L., Baghel, A., Radford, S. E., Frydman, J. & Deuerling, E. Dual Role of Ribosome-Binding Domain of NAC as a Potent Suppressor of Protein Aggregation and Aging-Related Proteinopathies. *Mol Cell* **74**, 729-741.e727, doi:10.1016/j.molcel.2019.03.012 (2019).

32 Allen, A., Gau, D., Francoeur, P., Sturm, J., Wang, Y., Martin, R., Maranchie, J., Duensing, A., Kaczorowski, A., Duensing, S., Wu, L., Lotze, M. T., Koes, D., Storkus, W. J. & Roy, P. Actin-binding protein profilin1 promotes aggressiveness of clear-cell renal cell carcinoma cells. *J Biol Chem* **295**, 15636-15649, doi:10.1074/jbc.RA120.013963 (2020).

33 Zou, Y.-h., Li, X.-d., Zhang, Q.-h. & Liu, D.-z. RACK1 Silencing Induces Cell Apoptosis and Inhibits Cell Proliferation in Hepatocellular Carcinoma MHCC97-H Cells. *Pathology & Oncology Research* **24**, 101-107, doi:10.1007/s12253-017-0214-6 (2018).

34 Zanni, G., Barresi, S., Travaglini, L., Bernardini, L., Rizza, T., Digilio, M. C., Mercuri, E., Cianfarani, S., Valeriani, M., Ferraris, A., Da Sacco, L., Novelli, A., Valente, E. M., Dallapiccola, B. & Bertini, E. S. FGF17, a gene involved in cerebellar development, is downregulated in a patient with Dandy-Walker malformation carrying a de novo 8p deletion. *Neurogenetics* **12**, 241-245, doi:10.1007/s10048-011-0283-8 (2011).

35 Zhang, S. & Cui, W. Sox2, a key factor in the regulation of pluripotency and neural differentiation. *World J Stem Cells* **6**, 305-311, doi:10.4252/wjsc.v6.i3.305 (2014).

1463 36 Concordet, J.-P. & Haeussler, M. CRISPOR: intuitive guide selection for
1464 CRISPR/Cas9 genome editing experiments and screens. *Nucleic Acids Research*
1465 **46**, W242-W245, doi:10.1093/nar/gky354 (2018).
1466 37 Yumlu, S., Stumm, J., Bashir, S., Dreyer, A.-K., Lisowski, P., Danner, E. & Kühn,
1467 R. Gene editing and clonal isolation of human induced pluripotent stem cells using
1468 CRISPR/Cas9. *Methods* **121-122**, 29-44,
1469 doi:https://doi.org/10.1016/j.ymeth.2017.05.009 (2017).
1470 38 Takasato, M., Er, P. X., Chiu, H. S., Maier, B., Baillie, G. J., Ferguson, C., Parton,
1471 R. G., Wolvetang, E. J., Roost, M. S., Chuva de Sousa Lopes, S. M. & Little, M. H.
1472 Kidney organoids from human iPS cells contain multiple lineages and model
1473 human nephrogenesis. *Nature* **526**, 564-568, doi:10.1038/nature15695 (2015).
1474 39 Kim, D., Pertea, G., Trapnell, C., Pimentel, H., Kelley, R. & Salzberg, S. L.
1475 TopHat2: accurate alignment of transcriptomes in the presence of insertions,
1476 deletions and gene fusions. *Genome Biology* **14**, R36, doi:10.1186/gb-2013-14-4-
1477 r36 (2013).
1478 40 Liao, Y., Smyth, G. K. & Shi, W. featureCounts: an efficient general purpose
1479 program for assigning sequence reads to genomic features. *Bioinformatics*
1480 *(Oxford, England)* **30**, 923-930, doi:10.1093/bioinformatics/btt656 (2014).
1481 41 Robinson, J. T., Thorvaldsdóttir, H., Winckler, W., Guttman, M., Lander, E. S.,
1482 Getz, G. & Mesirov, J. P. Integrative genomics viewer. *Nature biotechnology* **29**,
1483 24-26 (2011).
1484 42 Wagner, G. P., Kin, K. & Lynch, V. J. Measurement of mRNA abundance using
1485 RNA-seq data: RPKM measure is inconsistent among samples. *Theory in*

biosciences = Theorie in den Biowissenschaften **131**, 281-285, doi:10.1007/s12064-012-0162-3 (2012).